Anaesthesia disrupts mesoscale signal propagation in spite of enhanced responsivity in frontal but not in parietal cortex

Abhilash Dwarakanath[1,2,3,4], Majid Khalili-Ardali[1,5], Marion Gay[1], Raghuram HV[1,6], Maxime Roustan[1], Stanislas Dehaene[1,7], Bechir Jarraya[1,8,9], Theofanis I Panagiotaropoulos[1,10]

[1] Cognitive Neuroimaging Unit, INSERM, CEA, Université Paris-Saclay, NeuroSpin center, Gif/Yvette, France

[2] Neural Circuits and Cognition, European Institute of Neuroscience, Göttingen 37077, Germany

[3] Cognitive Neuroscience Laboratory, Perception & Plasticity Group, Deutsches Primatenzentrum, Göttingen 37077

[4] SFB 1528 Cognition of Interaction, 37077, Göttingen

[5] Donders Center for Neuroscience, Radboud University, Nijmegen, Netherlands

[6] Department of Psychology, University of Wisconsin-Madison, Madison, USA

[7] Collège de France, Université Paris-Sciences-Lettres (PSL), Paris, France

[8] University of Versailles Saint-Quentin-en-Yvelines, Université Paris-Saclay, Versailles, France

[9] Neuromodulation Unit, Foch Hospital, Suresnes, France

Corresponding authors - Abhilash Dwarakanath (ADwarakanath@dpz.eu); Theofanis Panagiotaropoulos (fpanag@psych.uoa.gr)

Summary

Understanding the effects of anaesthesia on cortical signal propagation at multiple spatiotemporal scales could provide insights into how cortical integration is disrupted during loss of consciousness. Non-invasive studies indicate reduced complexity of large-scale cortical patterns following perturbation of cortical activity under anaesthesia, compared to wakefulness. However, it is currently unknown how the cortex responds to local electrical microstimulation at the mesoscale during loss of sensory awareness, especially in higher order cortical areas believed to be involved in the emergence of consciousness. Using planar microelectrode arrays implanted in the ventrolateral prefrontal cortex (vlPFC) and posterior parietal cortex (PPC) of macaques, we simultaneously recorded and administered intracortical microstimulation at varying amplitudes during quiet wakefulness, as well as under light and deep sevoflurane anaesthesia. We found that the lateral spread rather than the strength of elicited cortical activity was consistently reduced under light and deep anaesthesia. Suppression of lateral signal propagation in the cortex could underlie a breakdown of mesoscale integrative processes during loss of consciousness, providing a novel mechanism for understanding cortical network effects of anaesthesia.

Corresponding authors ADwarakanath@dpz.eu; fpanag@psych.uoa.gr

Introduction

Consciousness, a fundamental aspect of human experience, encompasses a spectrum ranging from full awareness and altered states of consciousness to different levels of unconsciousness seen in anaesthesia and consciousness disorders[1–4]. Understanding the neural correlates of such unconscious states and the disruptive effects of these states on normal cortical functions, has significant implications for understanding the cortical mechanisms underlying conscious awareness, and for the treatment of consciousness disorders[5–7].

Multiple theoretical frameworks have been developed to address how consciousness arises in the brain [8,9]. Among the theories that ascribe a role to higher cortical and association areas [10–13; 14], the Global Neuronal Workspace Theory (GNWT) proposes that conscious experience arises from a higher-order cortical mediated ignition, amplification and widespread dissemination of sensory information across the brain, with the prefrontal cortex (PFC) playing a key role [15–18]. Multiple studies in humans conducted using non-invasive whole-brain recording techniques such as BOLD-fMRI have indeed implicated the PFC during conscious, accessible perception of a stimulus [19–21]. More specifically, direct electrophysiological recordings in the PFC show that prefrontal neuronal populations represent the contents of consciousness while ongoing low frequency fluctuations in the prefrontal state are involved in the stability and update of these contents [22–26].

The PFC is of particular interest due to its dense reciprocal connections with other cortical areas, especially the parietal cortex, forming a fronto-parietal loop (FP-loop)[27–30]. Crucially, apart from conscious perception, this frontoparietal network is believed to be central for sensory awareness that is disrupted under anaesthesia[15]. To address the role of these areas, in particular the ventrolateral prefrontal cortex (vlPFC) and the posterior parietal cortex (PPC) in the genesis and loss of conscious awareness, perturbational studies are necessary [10,31]. In particular, studying them under anaesthetics, which cause reversible unconsciousness, can help reveal mechanisms of consciousness loss and recovery [32–36].

Corresponding authors ADwarakanath@dpz.eu; fpanag@psych.uoa.gr

Different anaesthetics have been used to understand local and global neural dynamics during conscious and unconscious states [32,37]. For GABAergic anaesthetics, cortical states are dominated by anteriorised slow rhythms [38–42] in the delta-theta range (1-4 and 5-8 Hz)[43,44] exhibiting high intra-areal but low inter-areal coherence [40,43,45]. Sevoflurane, a commonly used veterinary inhalant anaesthetic, potentiates inhibitory neurotransmission, primarily enhancing $GABA_A$ receptor function[33,46]. Furthermore, sevoflurane reconfigures cortical neuronal discharge activity from diffuse and decorrelated, to distinct UP/DOWN states[47] with increased local neuronal correlations [33,48] while impairing functional connectivity [49–51]. Crucially, sevoflurane disrupts fronto-parietal communication [49,50] while also leading to a reduction in large-scale signal complexity (as measured by the Perturbational Complexity Index), a signature of the level of consciousness [32,52]. However, the exact nature of this functional reorganisation at the neuronal population level, in particular at the mesoscale, remains uncharacterised [53,54]. While studies have measured the complexity of large scale brain activity and distinct states elicited by transcranial magnetic stimulation (TMS) perturbation using scalp EEG [55,56], investigations specifically targeting nodes of the fronto-parietal loop to characterise the effects of loss of consciousness on mesoscale signal propagation are lacking.

This study aims to address three important questions at the mesoscale cortical level: (1) How does the response profile of prefrontal and parietal populations to electrical stimulation differ across awake and anaesthetised states? (2) How do these states affect signal propagation in time and space? (3) Are there differences in the thus inferred network properties between these two subunits of the FP-loop? To answer these questions, we employed a simultaneous electrical microstimulation-recording protocol during quiet wakefulness (QW), light (LS) and deep anaesthesia (DS), all performed in the same experiment and recording from the same population, to maintain sample consistency. The vlPFC and PPC were recorded in different animals and sessions. Apart from quasi-similar population response profiles in the two cortical regions, our results reveal a specific signature of anaesthesia in the PFC involving suppression of lateral electrical signal propagation, that is absent in the PPC. In contrast, the amplitude of responses following electrical microstimulation did not

Corresponding authors ADwarakanath@dpz.eu; fpanag@psych.uoa.gr

correlate with the level of anaesthesia since deep anaesthesia resulted in responses that were stronger compared to quiet wakefulness.

Results

We recorded and stimulated from the ventrolateral prefrontal cortex of two male macaques during quiet wakefulness and anaesthesia, in the same experimental sessions, using a 10 x 10 Iridium Oxide coated Utah Array. Specialised adapters allowed us to stimulate and record members of the same population, simultaneously (Fig. 1A).

After recording and electrical microstimulation periods during quiet wakefulness, we induced anaesthesia with a single injection of ketamine and dexmedetomidine. After waiting for ~90 minutes for the ketamine to metabolise, light anaesthesia was induced by inhalation, and maintained between 1-1.5% of sevoflurane, a GABAergic anaesthetic. After recording and microstimulation during light anaesthesia, we increased the sevoflurane concentration to 3%, inducing deep anaesthesia (Fig. 1B). While most intracortical microstimulation (ICMS) that intend to characterise population response properties employ single-pulse stimulation, we devised our stimulation to mimic those used in studies that seek to, for e.g., augment stimulus detection, or influence behavioural outcome [57–60]. This stimulation, designed as a biphasic 50-pulse train at 250 Hz, was delivered to the two electrodes in the centre of the array, each with opposing polarity, at varying strengths, viz. 1 to 100µA (Fig. 1B). Each stimulation was spaced 10-20s apart to allow sufficient time for cortical activity to return to baseline activity post-stimulation. Resting state periods, both during wakefulness and anaesthesia, were recorded in pre- and post-stimulation periods (Fig. 1C).

State characterisation in wakefulness and different anaesthesia depths

How does the activity of the same cortical population vary between quiet wakefulness and different levels of anaesthesia?

Corresponding authors ADwarakanath@dpz.eu; fpanag@psych.uoa.gr

To address this, in each session from each recorded area in each animal, we selected a population of neurons based on their firing rate during QW (firing rate >= 0.5 spks/s), and used the same population for all downstream analyses. In Monkey A in the PFC, while the firing rates during LS and DS were significantly lower than during QW ($p_{Comp} < 0.001$), they were not different from each other ($p_{Comp} > 0.05$). In Monkey C in the PPC however, there were significant differences in the firing rate between QW and DS, and LS and DS ($p_{Comp} < 0.001$), but not between QW and LS ($p_{Comp} > 0.07$). In general, the firing was higher during QW, followed by LS and then DS, subject to statistical tests as above. In Monkey B in the PFC, due to very sparse firing, no significant differences were found in the firing rates between any of the 3 conditions (all $p_{Comp} > 0.5$). The firing rate comparisons are summarised in SIFig. 1. Because each session contained the same number of channels recorded, for this statistical comparison, the Student's t-test was employed.

Qualitatively, quiet wakefulness is typified by neuronal discharge activity which is diffuse and uncorrelated between channels (Fig. 2A (PFC) and Fig. 2E (PPC) - top row), accompanied by low amplitude high frequency field fluctuations (gamma) (Fig. 2C (PFC) and 2G - top row). The induction of anaesthesia leads to a transition from this decoherent state to periods of coherent discharge interspersed by silence, known as UP/DOWN states, possibly leading to burst suppression in DS (Fig. 2A (PFC) and Fig. 2E (PPC) - middle row (LS), and bottom row (DS)) [47,61]. This is reflected in significantly lower delta-theta power, and significantly higher beta and gamma power during wakefulness ($p_{Comp} < 0.0001$; SIFig. 2), whereas both states of anaesthesia are dominated by low-frequency field activity (Figs. 2D (PFC), 2H - PPC). In both recorded areas, the power in the low-frequencies increased with increasing depth of anaesthesia (LS vs DS; $p_{Comp} < 0.0001$; SIFig. 2).

We quantified the observed pattern of activity during these resting state periods (in both wakefulness and two levels of anaesthesia) using a two-state Hidden Markov Model (HMM) fit to the population firing vector. From the learned state sequence, the durations of bursting (UP) and silent (DOWN) periods were computed. While the model did not fit wakefulness well (Fig. 2A and 2E top row - purple line P(UP)), indicating the absence of such states during this period, it detected UP/DOWN states reliably in both LS and DS, in both PFC and PPC (Fig 2A and 2E, middle (LS) and

bottom (DS) rows). While in Monkey A (PFC) and Monkey C (PPC), DS was typically characterised by long silent periods up to ~16s (PFC, Fig. 2I Column 1) and ~100s (PFC, Fig. 2I column 3), silent periods in both LS and DS were restricted to ~2.6s in Monkey B (PFC, SIFig. 3)

Finally, a synchrony index (SI) computed from the positive half of the autocorrelation function (ACF) excluding the peak suggests that while synchrony of population firing is relatively high during both LS and DS periods, QW displays low synchrony (Fig. 2B (PFC) and 2C (PPC); SIFig. 1), in both the PFC and the PPC. The difference in synchrony between each state was evaluated statistically, and all differences were significant with all $p_{Comp} < 0.001$. We attribute this to the coherent UP/DOWN states observed under anaesthesia.

State dependence of cortical responsivity to electrical microstimulation

Following the characterisation of prefrontal and parietal states during wakefulness and different depths of sevoflurane anaesthesia, we examined the pattern of cortical response to electrical microstimulation administered at the centre of the implanted Utah array during these different states. Trial and channel averaged peri-stimulus time histograms (PSTHs) for spiking activity (Figs. 3A - PFC & 3C - PPC), and the same for LFPs (0.1 to 250Hz) (Fig. 4A - PFC & 4C - PPC) were computed aligned at stimulation offset.

For lower microstimulation amplitudes viz. 1, 5 and 8 μA, the baseline-normalised spiking activity displayed a suppression during the microstimulation period, followed by a sharp excitatory transient immediately after the end of microstimulation for all consciousness states (QW, LS and DS), in both PFC and PPC. Perhaps counterintuitively, the excitatory transient was stronger in amplitude for DS compared to QW and LS, in both recorded regions. However, for higher amplitudes (15-25 μA), we observed a different pattern present again in all consciousness states. In the PFC, spiking activity increased during the microstimulation period, which was then followed by a period of long-lasting inhibition (~1-1.5seconds), finally bookended by a later rebound. This rebound was the lowest during light anaesthesia, and highest

during deep anaesthesia in the PFC (Fig. 3A). Interestingly, while only one rebound occurred in the PFC, two rebounds manifested in the PPC, with the inhibition and rebound occurring faster and lasting for a shorter time (Fig. 3C). Furthermore, both the transient and the rebounds in the PPC followed a gradient according to the state, i.e. DS > LS > QW.

The above-mentioned characteristics are summarised as violin distributions (Fig. 3B - PFC, and Fig. 3D - PPC), estimated using an n-peak detection algorithm. In the PFC, for the lower stimulation amplitudes, the response during QW was the fastest, followed by during DS, with the slowest response manifesting during LS (Fig. 3B). However, in the PPC, the response occurred earlier in LS than during QW, with DS being the fastest. (Fig. 3D). Furthermore, the strength of the responses was highest during DS, which can potentially be attributed to increased cortical membrane sensitivity during burst suppression periods [62,63]. While in the PFC, the response and rebound strengths were weakest during LS, with DS being the highest, in the PPC, again, the response strength showed an increasing trend with anaesthesia. The mean occurrence times, their strengths, and their dispersal, under QW, LS and DS, for both Monkey A (PFC) and Monkey C (PPC) are catalogued in SI Table 1 (PFC) and SI Table 2 (PPC), along with confidence intervals (CIs) for the difference in means (If a CI includes 0, then no significant differences between the two states are seen).

The LFPs also displayed stimulation-dependent heterogeneity in the response pattern and strength, both in the PFC (Fig. 4A) and the PPC (Fig. 4C). For lower amplitudes (1, 5 and 8 μA), following stimulation offset, a negative deflection is seen, often followed by a positive rebound. However, these responses are noisy (Fig. 4C insets), and highly variable. For higher amplitudes (15-25 μA), following stimulation offset, a strong positive deflection is elicited followed by a delayed negative dip. These responses are highly stereotypical and consistent (Fig. 4C insets). While the first transient happened earliest during QW, and latest during DS, the reversal occurred latest during QW and earliest during DS, in both the PFC and the PPC. Furthermore, the initial response transient was sustained for the longest time (peak width duration) during QW, while it resolved itself the fastest during LS, pointing to its role in modulating membrane potentials of the constituent neurons of the population in the slow rhythm range (~0.5-2Hz; data not shown). The mean occurrence times, their

strengths, and their durations, along with their dispersal, under QW, LS and DS, for both Monkey A (PFC) and Monkey C (PPC) are catalogued in SI Table 3 (PFC) and SI Table 4 (PPC) respectively, along with confidence intervals (CIs) for the difference in means (If a CI includes 0, then no significant differences between the two states are seen).

In summary these results show that causal perturbation via targeted electrical stimulation elicits state, stimulation strength, and space dependent heterogeneity in the response activity of the fronto-parietal network.

Spatiotemporal modulation of prefrontal activity in different consciousness states

To study whether the state of consciousness has an effect on lateral signal propagation in the two cortical regions, the electrodes on the Utah array were binned according to their distance from the stimulated electrodes in 0.4mm bins, from the nearest (0.4 to 0.8mm) to the farthest (2-2.4mm in PFC and 2.4-2.8mm in PPC). Responses to ICMS were pooled for all stimulation amplitudes in Monkey A and Monkey C, while in Monkey B, only the response to 15 µA stimulation was analysed (only 2 amplitudes were tested in Monkey B viz.15 and 100 µA. 100uA displayed complete suppression in Monkey B, and thus was discarded from the analysis). The field response profiles by distance to the stimulated electrode are displayed in Fig. 5A (PFC) and 6A (PPC) respectively, with 2 stimulation amplitudes being represented, viz. 8 and 15 µA.

Because of the distinct response patterns to the low and high amplitude regimes elicited in the spiking activity, viz. a simple transient excitation versus a transient followed by inhibition, and rebound, in both the PFC and PPC, we restricted the analysis of the spatial modulation of population activity to the LFPs.

LFP signal energy modulation over distance were computed as the normalised pre/post change in activity in a 4s bin following the end of stimulation. The signal response was modulated strongest during QW, displaying non-monotonicity over distance, while they were modulated the least during DS, and decreased sharply over distance (Fig. 5B). Neuronal activity in LS displayed modulation strength in between

QW and DS, and also decayed linearly over distance, albeit slower than DS (Fig. 5B). This points to a maintenance of the strength of modulation at longer distances during QW, with proximal and distal populations being modulated equally, while signal propagation is restricted with increase in distance, in both states of anaesthesia. These are confirmed by the analysis of the sum of the rate of change over distance, combined with a Bayesian bootstrapped comparison-of-means. The spatiotemporal characterisation for Monkey B is presented in SI Fig. 4.

In the PPC however, modulation decreased with distance in all three states pointing to no non-monotonic recovery of signal propagation with distance (Fig. 6B). However, as opposed to the PFC where in the LFPs, the strongest modulation was observed during QW (Fig. 5B), in the PPC, the strongest modulation was seen in the DS.

A 0.5s bin by bin analysis of this modulation in time in the PFC, starting immediately after stimulation offset, displays the preservation of this non-monotonicity during wakefulness (Fig. 5C; Left Column), even up to 6s after stimulation offset, in the LFPs. However, during both levels of anaesthesia, the drop off of signal energy modulation over distance remained in all time bins (Fig. 5C Middle and Left Columns). In the PPC, the decay in time was even faster, strong excitatory modulation extinguishing already after ~2.5s (Fig. 6C).

Taken together, our results suggest that the prefrontal cortex not only displays distinct differences in responses in spiking activity and LFPs to electrical microstimulation, it also displays differential responsivity to low and high amplitudes of stimulation, under different states of (un)consciousness. Most importantly, our data show that while field signal propagation in the PFC is starkly reduced under anaesthesia, as compared to wakefulness, only the strength of modulation displays significant differences between the states in the PPC.

Discussion

The PFC exhibits a rich diversification of structure [64–66], and consequently, function. It serves as an integrative hub for a multitude of cognitive processes such as

inhibitory control, decision making, cognitive control, working memory, and the integration of sensory information with planned actions [67–73]. Under anaesthesia, both rodent and human studies have revealed notable alterations in PFC activity. Specifically, anaesthesia has been shown to induce a transition from desynchronised to highly synchronised oscillatory activity in the PFC of rodents [54,74,75]. In humans, anaesthetic agents have been observed to disrupt functional connectivity within the PFC, which correlates with a decline in conscious awareness and cognitive function [76–78]. Pressingly, what can we learn from characterising macaque PFC population dynamics by monitoring and perturbing neuronal populations during these (un)conscious states?

Altered mesoscale cortical dynamics under anaesthesia

Multiple previous studies have monitored cortical populations across the dorsal and ventral pathways in different animal models during rest. Furthermore, global dynamics have been studied using gross-scale techniques in humans. Perturbational studies in humans and monkeys under different (un)conscious states have been performed with both DBS and TMS [56,79–82]. However, to date, consistent, simultaneously-recorded mesoscale cortical populations in different states have not been monitored, and perturbed.

We show that chaotic and dispersed spiking activity in the same population during the awake state reorganises into coherent UP/DOWN states during anaesthesia, both during light and deep anaesthetic states (Fig. 2). The distinguishing feature between LS and DS both in the PFC and PPC seems to be a long tail of the duration distributions of the down states during DS (Fig. 2), thus signifying a quieter, i.e. less active cortex. However, a higher population synchrony in DS agrees well with the significantly larger low-frequency power (Fig. 2, delta and theta), and therefore coherence (data not shown). These long periods of cortical silence, termed burst suppression in neurological EEG literature, could reset cortical responsivity during anaesthesia at the mesoscale.

Response characteristics of the PFC and PPC

Corresponding authors ADwarakanath@dpz.eu; fpanag@psych.uoa.gr

In the past, a majority of causal perturbational studies have been used either to bias perception and behaviour by stimulating stimulus-selective neurons in sensory cortices [57,83–86] [87] or object recognition areas [88] , or for brain computer interfaces (BCIs) [89], and therapeutic purposes [90–92]. While studies that electrically and pharmacologically perturb the PFC in humans [31,93] and animal models [10,94] exist, they are sparse and not systematised, neither in the behaviour or sub-behavioural range, nor under different arousal states. Our study addresses this *lacuna* specifically with respect to intracortical microstimulation by assaying the primate higher associational cortices. Crucially, no studies exist that simultaneously monitor and perturb the same consistent population of prefrontal and parietal neurons under different states of consciousness, thus targeting the fronto-parietal loop.

Our results (Figs. 3A and 3B) suggest the existence of two membrane-responsiveness regimes with respect to electrical challenge in these cortical populations. We show that low amplitude stimulation seems to display an initial inhibition followed by excitation (Fig. 4A - Left). However, large current injections elicit first a strong transient, followed by a long-lasting inhibition, after which the spiking activity rebounds with a vengeance (Fig. 4A - Right). Inhibitory neuronal populations, though comprising only 15-30% of the cortex [95,96], tightly regulate microcircuit function [97,98]. Post-inhibitory rebound and its relationship to recurrent inhibition is widely-known in a variety of intrinsically and extrinsically-driven contexts [99]. Large current insults could reflect a disruption of this inhibitory control, and its subsequent release, pointing to an inhibitory population led network reorganisation [100,101]. This heterogeneity, also preserved in the LFPs (Figs. 4A and 4B), could therefore point to downstream perisynaptic modulation, allowing the cortical membrane potential to display differential activity as a consequence.

In the PPC, in addition to the transient-inhibition-rebound, we observe a second rebound that happens very close to the first (Fig. 3C). Because the firing rate before this rebound does not return to baseline, and instead manifests as a “second peak”, this extra rebound could potentially arise from recurrent excitation, and could be crucial in self-generated and sustained neural activity, that can be broadcasted to organise on-line circuit control [102,103].

Corresponding authors ADwarakanath@dpz.eu; fpanag@psych.uoa.gr

The responsivity paradox

Our data also indicate that fronto-parietal responsivity is highest during deep anaesthesia. What seems at first paradoxical, lends itself to a remarkable interpretation in terms of equilibrium dynamics. During deep anaesthesia, long periods of iso-electric voltage lines (in the EEG) interspersed with brief, large fluctuations exist (Fig. 2A), which is termed "burst suppression" [104]. We speculate that during these extended periods of cortical silence, the neuronal membrane is hyper-sensitive [62], thereby allowing it to return to equilibrium, during which, any reasonably strong perturbation could potentially push the system into an accelerated, hyperbolic trajectory, manifesting as fast and strong responses. Such empirically-determined cortical activity patterns under perturbation, rest and different states are imperative for constraining models of brain function at multiple scales.

Contrasting resting state activity profiles with the observed response dynamics underscores the potential limitations in inferring the exact state of consciousness (for e.g., depth of anaesthesia) from temporal patterns in population activity. Despite the varying distributions of quiescent intervals across sessions and subjects, the pattern of increased responsivity coupled with limited spatial propagation during deep sedation (DS) was a consistent finding. This observation is bolstered by the analysis of proximity to criticality (see SI. Fig 1), which showed uniform spatial and temporal response characteristics across sessions and subjects, regardless of any significant shifts in criticality between light sedation (LS) and DS.

Moreover, the hypothesis that direct stimulation may induce prolonged suppression, culminating in a synchronised and markedly amplified rebound, suggests that during DS, complexity indices—evaluated through methods like perturbational complexity index (PCI) and pattern analysis—would be reduced due to this enforced, homogenous, and intensified rebound effect. Consequently, beyond a certain depth of anaesthesia, where neuronal populations reach a threshold of inhibitory saturation, a progressive decline in criticality or complexity metrics may not be evident. In effect, these metrics potentially only reflect this specific inhibitory population led dynamics, rather than a true reconfiguration of information, and thus complexity. Future investigations could explore these dynamics through BOLD-fMRI under varied

Corresponding authors ADwarakanath@dpz.eu; fpanag@psych.uoa.gr

anaesthetic conditions and DBS protocols, coupled with advanced PCI evaluations using complex TMS protocols, including pulse-train stimulation, to thoroughly examine and correlate activities across different scales.

Signal communication is maintained during wakefulness in PFC but not in PPC

Anaesthesia is speculated to induce unconsciousness in many ways [32,45,105], a primary one among which is by suppressing information processing and communication. This is evidenced by global inhibition, i.e. the reduction in neuronal spiking activity [106,107]. Additionally, local synchrony increases but global synchrony has been observed to be disrupted under anaesthesia [108], while during wakefulness, although locally neurons remain uncorrelated in their firing, large-scale synchrony is observed across brain regions [109–111], specifically with the persistence of the Default Mode Network (DMN) [112]. This change in synchrony patterns under anaesthesia suggests a disruption in normal information processing in the brain, which at the prefrontal cortical level is confirmed by our results.

Crucially, the dorsal and ventral PFC have been shown to contain features that distinguish them from lower cortical regions [113]. For example, instead of distinct organisation into cortical columns, the PFC instead shows greater lateral connectivity among distributed pools of functionally distinct neuronal cell types [114 115 65 116]. Layer 5 pyramidal neurons project out of the cortex and receive extra-cortical and subcortical efferents to establish overarching connectivity [117,118.119]. Long-range fronto-parietal connections exist which form the fronto-parietal loop, a unit central to the GNW [14,16,120]. Most importantly, the PFC displays not only abstract tuning such as task-phase [121], but also stimulus features [122]. These various modes of differentiation and integration [123] are ideal for complex information processing, such as those required for conscious awareness [13 124]. A unique and computationally significant property of neuronal networks is functional connectivity, which can be measured using noise correlations at the mesoscale [125,126]. The structure of this functional connectivity in lower cortical areas is a linear decrease with lateral distance, both under wakefulness and anaesthesia, whereas in the PFC it is non-monotonic, showing that proximal and distal populations are equally connected [127,128]. This is also evidenced by patchy

anatomical connectivity between pools of excitatory and inhibitory populations [65,114,116,129]. This unique pattern of connectivity in the PFC suggests that it can be used for complex integrative functions [69,130–132] that lower order areas cannot perform. Interestingly, primary sensory areas, with the exception of the somatosensory cortex, aren't much perturbed during anaesthesia, even at deep levels [133] [134]. These observations lend support to the hypothesis that loss of consciousness is triggered by a lack of higher-order integration in the cortex [135] [50]. Lower areas don't need long-range functional connectivity because they process low-level stimulus features independently and don't need to integrate. However, feature-binding (Gestalt) is necessary for conscious perception [136–140], the PFC being a prime candidate [141–143].

From the standpoint of GNW, although the PPC is indeed part of the fronto-parietal loop[77], and distinct patterns of directionality, strength and functional organisation are observed across states of consciousness in each individual module of the loop[77,144], it is the PFC that is supposed to amplify, broadcast and coordinate brain-wide activity to allow for consciousness to emerge[15,17]. Therefore, we posit that anaesthesia must necessarily disturb the PFC, not that it is only sufficient to dampen PFC or PPC activity. If anaesthesia causes an information bottle-neck, long-range coordination of neuronal activity by an orchestrating node would become weak or impossible. Our results (Fig. 5) show – that although fast spatial spread of global activity in V1 is seen immediately post ignition – that strong horizontal connectivity and lateral information flow, only in the PFC, is a signature of conscious wakefulness and indeed breaks down under anaesthetic unconsciousness, suggesting that such complex functional cytoarchitecture in frontal regions is necessary for integrative processes crucial to conscious awareness, which subsequently implicates its disruption in loss of consciousness.

Causal perturbation of the fronto-parietal circuit and its systemic implications

In the ongoing discussion surrounding the role of the PFC in consciousness and DoCs, studies employing intracranial electrical stimulation (iES) to causally perturb networks of interest have recently begun to not only provide unique, unexpected and contradictory insights [93], but also elicit spirited debate [31]. Most importantly, studying

cortical response properties under external stimulation can help elucidate the mechanistic underpinnings of consciousness, as opposed to purely correlative studies. Causal perturbational studies are crucial as they allow for the manipulation of specific neural populations, thereby providing direct evidence of their role in consciousness. To even begin to design appropriate experiments addressing this large gamut of questions, it is vital that a foundation is securely built on thorough electrical and optical characterisation of these mesoscale networks. Furthermore, insights gained from such studies can be used to constrain larger neuronal models of cortical activity under different states of consciousness.

Studies employing iES or ICMS in animal models have also provided indirect support for a central role of the PFC in conscious awareness. For example, it has been shown that when the primary visual cortex (V1) is stimulated, correct detection trials consistently display sustained PFC activity as opposed to misses [58,59]. In terms of the state of consciousness, a landmark study in rodents demonstrated robust RoC after carbachol injection to the PFC, but crucially, not the PPC [10]. Interestingly however, when the thalamus is stimulated using deep brain stimulation (DBS) to arouse the experimental subject, both the PFC and the PPC are strongly activated, indicating the engagement of fronto-parietal populations during RoC [145–147]. In task contexts for instance, global deviants in the local-global task [148], which are a signature of conscious access, can then be decoded from the PFC when other behavioural signs of arousal re-manifest [145]. DBS has also shown promise in "enhancing" conscious access in patients with minimally conscious state (MCS), marking a significant advancement in DoC intervention [79]. These findings trace a functional link between the thalamic relay and higher associational populations in conscious access, potentially engaging a broader thalamo-cortical circuit, thereby restoring consciousness in patients with DOCs, while also providing a more nuanced approach in identifying potential therapeutic targets, such as cautiously employing direct cortical stimulation - rather than strongly invasive and high-strength DBS - could. However, systematic protocols for characterising ICMS effects during wakefulness or anaesthesia (as a proxy for DoCs) are lacking. Our study attempts to fill this gap by exploring myriad stimulation protocols and parameters (Fig. 1).

Limitations

In our study, we recorded stable prefrontal and parietal populations during all states of (un)consciousness. However, it is prudent to note that the PFC and PPC data come from two different animals, due to the unfortunate loss of the PFC and the PPC array in each animal respectively (in the other animal, no spiking activity could be recorded from the PPC array). This inherently limits the direct comparison of the two areas forming the frontoparietal loop. However, it is our firm belief that the consistency of responses and functional modulation over space and time seen in our data would predict the same across simultaneous recordings too.

Furthermore, since we used stimulation regimes that have previously been shown to elicit behavioural responses [58,59,149–151], we did not probe the cortex classically with single-pulse stimulation, as our goal was to also investigate response characteristics and signal spread under these un(conscious) states.

Conclusion

Taken together, our results reveal that the PFC and the PPC exhibit unique and intriguing responses when subjected to electrical stimulation, specifically shedding light on the putative functional role of the PFC in regulating states of consciousness. Most importantly, we show the restriction of lateral signal propagation under anaesthesia in the PFC, which could result in break-down of crucial integrative processes that are necessary for consciousness and cognition. These results can further significantly inform and constrain cortical models of brain function in health and disease.

Further investigation into the effects of elevated electrical stimulation intensities on these higher order association areas offers a promising avenue for future research. By delving into the consequences of stimulation whose parameters are in the range to elicit behavioural effects, we have the opportunity to elucidate the nuanced relationship between PFC activity and specific behavioural metrics, particularly in arousal and its loss. This line of enquiry holds substantial clinical implications, especially for individuals afflicted with DoCs. Given that our current stimulation design did not demonstrate behavioural signs of arousal or long-range cortical excitability, we hypothesise that higher stimulation intensities or alternative

stimulation patterns, as guided by dynamic brain activity [83,152,153], could potentially increase cortical excitability and thus awaken subjects under anaesthesia. To this end, we are initiating further studies aimed at assessing the feasibility of reversing anaesthesia-induced unconsciousness through targeted electrical stimulation of the frontoparietal loop.

Figure Captions

Figure 1 | Experimental design and ROI

A. Multielectrode array in the inferior convexity of the PFC, thus targeting the fronto-parietal loop, placed anterior to the bank of the arcuate sulcus and below the principal sulcus, thus being localised to the left ventrolateral prefrontal cortex

B. Cortical population activity was recorded in four experimental phases, viz. Quiet wakefulness (QW), transition to anaesthesia and preparation, light anaesthesia (LS - 1-1.5% Sevoflurane), and deep anaesthesia (DS - 3% Sevoflurane), along with the delivery of intracortical microstimulation. The stimulation was devised as a train of 50 biphasic pulses lasting 200ms, with varying amplitudes, presented randomly with an inter-stimulation interval between 10-20s.

C. At the start of each experimental epoch, 15-20 mins of resting state activity was recorded, followed by the three stimulation regimes, viz. Centre-array stimulation, full-array stimulation, and full-array high-frequency, high-amplitude stimulation, finally followed by 15-20 mins of post-stimulation resting state.

Figure 2 | PFC and PPC display distinct neuronal population activity patterns under different conscious states

A. PFC - Reorganisation of spiking activity into periods of UP and DOWN states in anaesthesia (LS - Green, DS - Blue) as compared to desynchronised activity during QW (Red). DS also displays extended periods of cortical silence (seconds to minutes) termed “burst suppression”.

B. PFC - Autocorrelograms of the population firing vector computed in chunks. While LS shows a wider peak, the strength of the non-shifted correlation is highest during DS and lowest during QW.

C. PFC - z-scored time-frequency wavelet decomposition of the corresponding LFPs. While QW is identified by its characteristic ongoing high-frequency power which follows spiking, this is suppressed during both types of anaesthesia, where slower rhythms dominate. The purple line indicates the learned UP state path from the 2-state HMM. *n.b.* - Shown is one example period from Monkey A.

D. PFC - z-scored spectrum for the example epochs. While all frequencies are well-represented during QW, especially beta and gamma, during LS and DS, the spectral activity is concentrated in the 0.1-8 Hz range.

E, F G and H depict the same as above, but for the PPC.

I. Col 1 & Col 2 - Duration of DOWN and UP states in the PFC. Col 3 & Col 4 - Duration of DOWN and UP states in the PPC. Green is LS, Blue is DS. While during both LS and DS, the durations of the up states stay below 3s, the durations of the silent periods extend to 15s (PFC) and 100+s (PPC) during DS.

Figure 3 | Spiking characteristics

A. Peri-stimulus time histograms (PSTHs) computed for all stimulation amplitudes (1, 5, 8, 15, 20, 25μA) during QW, LS and DS, in the PFC. The firing rates were averaged over channels and trials, and aligned to stimulation offset. Insets are zoomed in on the response shape.

B. This panel characterises the above activity as violin distributions, estimated using an n-peak detection algorithm. It represents the times at which the peak transients and rebound occurred. While the cortical population response to low amplitude stimulation is temporal fast, transient, and exhibits an initial inhibition followed by excitation, higher amplitudes elicit an initial transient followed by long lasting inhibition, after which the discharge activity rebounds.

C. Same as A, for PPC.

D. While the cortical population response to low amplitude stimulation is temporal fast, transient, and exhibits an initial inhibition followed by excitation, higher amplitudes elicit an initial transient followed by short inhibition, after which the discharge activity rebounds, followed by another rebound. This does not occur in the PFC.

Figure 4 | LFP characteristics

A. LFP activity for all stimulation amplitudes (1, 5, 8, 15, 20, 25μA) during QW, LS and DS, in the PFC. Insets are zoomed in on the response shape.

B. This panel characterises the above activity in terms of the timing of the induced up or down state post stimulation. While the cortical population response to low amplitude stimulation first elicits a negative deflection followed by a positive overshoot, this pattern is reversed for higher amplitudes.

C. Same as A for PPC

B. Same as B for PPC

(*n.b.* - In both the LFPs and neuronal discharges, the heterogeneous response patterns can be grouped into two distinct groups, viz. those in response to "low" amplitudes (1,5,8 μA) and those in response to "high" amplitudes (15, 20, 25 μA).)

Figure 5 | Modulation of cortical information flow in different states - PFC

A. Shows the average LFP response aligned to stimulation offset in the three states, viz. quiet wakefulness, light and deep anaesthesia, for two example amplitudes from each regime, i.e. "low" and "high" stimulation, sorted by distance, from nearest (0.4mm) to farthest (2.6mm) nodes from the centre. As noted previously, stimulation was delivered to the two centre electrodes.

B. Whereas during QW, proximal and distal populations show similar modulation of field activity, this modulation falls off over space during both types of anaesthesia, with

the decrease being stronger during DS (Insets show the sum of the first derivative for the proximal and distal populations). Data points show the mean and SEM.

C. Top - Shows the evolution of field signal energy modulation in 0.5s bins starting immediately after stimulation offset, until 7s after stimulation. While the non-monotonicity is preserved in almost all time bins during QW, it does not manifest during LS or DS at all, showing a lack of spatial spread of information.

Figure 6 | Modulation of cortical information flow in different states - PPC

A. Shows the average LFP response aligned to stimulation offset in the three states, viz. quiet wakefulness, light and deep anaesthesia, for two example amplitudes from each regime, i.e. "low" and "high" stimulation, sorted by distance, from nearest (0.4mm) to farthest (2.8mm) nodes from the centre. As noted previously, stimulation was delivered to the two centre electrodes.

B. Field signal energy modulation in the PPC shows that no non-monotonic structure is observed at all in the LFPs in the PPC, as opposed to the PPC. Furthermore, As opposed to the PFC, in the PPC, DS modulation remains higher than QW and LS.

C. While the strength of modulation persists for longer after stimulation in the PPC during QW, it extinguishes fastest during LS, and then DS. No non-monotonic structure is observed in any time-bin in any state after stimulation.

Acknowledgments

We thank Dr. Lynn Uhrig for her assistance with anaesthesia. We are thankful to Jeremy Bernard for assistance with the custom-made setup for the experiment. We would also like to thank Prof. Dr. B S Dwarakanath for helpful discussions and comments, and proof-reading assistance.

Author contributions

Conceptualisation: AD, TIP ; Data curation: AD; Formal analysis: AD; Funding acquisition: BJ, SD, TIP ; Investigation: AD, MKA, MG, MR, RHV, BJ, TIP;

Methodology: AD, MKA, RHV, TIP; Project administration: TIP; Resources: MG, MR, BJ, SD, TIP (lead); Software: AD; Supervision: BJ, TIP (lead); Visualisation: AD (lead), RHV (supporting); Writing - original draft: AD; Writing - review & editing: AD, MKA, MG, MR, RHV, BJ, TIP (lead).

Funding

This work received funding from Inserm (BJ), CEA (TIP), Collège de France (SD), the European Union's Horizon 2020 Framework Programme for Research and Innovation under the Specific Grant Agreement No. 945539 (Human Brain Project SGA3, T2.10; TIP), a grant from Templeton World Charity Foundation, Inc (TWCF0562) to TIP, and a grant from the Bettencourt-Schueller Foundation to BJ.

Declaration of interests

The authors declare no competing interests.

STAR Methods

1. Resource availability

Information and requests for data and specific code should be directed to and will be fulfilled by the lead contact or the first author –

Theofanis I Panagiotaropoulos - theofanis.panagiotaropoulos@cea.fr (lead contact); Abhilash Dwarakanath - abhilash.dwarakanath@cea.fr

2. Materials and availability –

Not applicable

3. Data and code availability –

Electrophysiological recordings used in this paper will be used in the future for other studies. Therefore, the data is available upon reasonable request; please contact the lead contact. Custom stimulation, data acquisition and extraction, preprocessing,

and analysis scripts written in MATLAB are available on the first author's GitHub - (https://github.com/abhilashdwarakanath/IntracorticalMicrostimulation, https://github.com/abhilashdwarakanath/-Un-ConsciousStates, https://github.com/abhilashdwarakanath/EphysPreprocessing).

The data used in this manuscript will be made available through the Human Brain Project's EBRAINS Knowledge Graph, as a contribution from SGA3's Task 2.10.

4. Experimental model and subject details –

Two adult, male rhesus macaques (*Macaca mulatta)*, weighing between 10-12kg were recruited for the experiments. The subjects, denoted as Monkey "A" and Monkey "J", were pair-housed in an enriched animal facility. They were trained to be chaired and head-posted in the recording chamber.

5. Methods details -

Electrophysiological recordings

We performed extracellular electrophysiological recordings in the inferior convexity of the lateral PFC of 2 awake and anaesthetised monkeys using chronically implanted Utah microelectrode arrays[154] (Blackrock Microsystems, Salt Lake City, Utah USA). We implanted the arrays 1 - 2 millimetres anterior to the bank of the arcuate sulcus and below the ventral bank of the principal sulcus, thus covering a large part of the inferior convexity in the ventrolateral PFC, which forms one node of the fronto-parietal loop. The arrays were 4x4mm wide, with a 10 by 10 electrode configuration and inter-electrode distance of 400µm. Electrodes were 1mm long therefore recording from the middle cortical layers. The monkeys were implanted with form-specific titanium head posts on the cranium after modelling the skull based on CT scans. All experiments were approved by the local authorities' ethical committee (Protocol # - A18_028), and were in full compliance with the guidelines of the European Community (EUVD 86/609/EEC) for the care and use of laboratory animals.

Data acquisition and stimulation

Broadband neural signals (0.1–30 kHz) were recorded using Neural Signal Processors (NSPs) from Blackrock Microsystems Inc. Signals from the Utah array were digitised, amplified, and then routed to the NSPs for acquisition. The digitisation occurred on a CerePlex M Headstage which, coupled with Omnetics Y adapters, allowed us to simultaneously record and stimulate from the same electrodes. A CereStim 96 microstimulator from Blackrock Microsystems driven by MATLAB (2022a, MathWorks Ltd) code interfaced with their proprietary API was used to provide biphasic pulses between 1 to 210μA.

For the offline detection of action potentials, broadband data were filtered between 0.6 and 3 kHz using a second-order Butterworth filter (the filter was chosen such that it allowed a flat response in the passband while contributing the least phase distortion due to its low order, yet having an acceptable attenuation in the stop band, i.e. a roll-off starting at -20dB). The amplitude for spike detection was set to five times the median absolute deviation (MAD)[155]. Spikes were rejected if they occurred within 0.5 ms of each other, (multi-unit refractory period temporal threshold) or if they were larger than 50 times the MAD. Finally, all spikes that occurred at the same time point (within 3 samples at 30kHz) in a minimum of 60 channels (out of 96) were also discarded to exclude stimulation artefacts. All collected spikes were aligned to their minimum. For the analysis of LFP activity, the broadband signal was decimated to 500 Hz sampling rate using a Type I Chebyshev Filter, reliably preserving frequency components up to 200 Hz.

Experimental design

The animal was chaired and head-posted in the recording chamber, after which the eye-recording camera was aligned and centre-calibrated. The CereStim module was connected to the CerePlex M headstage for stimulation delivery, which was subsequently connected to the pre-amplifiers, which fed the recorded and referenced signals to the Neural Signal Processor (NSP) via fibre-optic cables.

The experiment consisted of four distinct phases viz. Quiet wakefulness (QW), induction and transition to anaesthesia, light anaesthesia (LS) and deep anaesthesia (DS). Each of the QW, LS and DS phases started with an initial recording of 15-20 mins

Corresponding authors ADwarakanath@dpz.eu; fpanag@psych.uoa.gr

of spontaneous activity. Next, multiple repeats (10 to 25) of a pulse train consisting of 50 pulses of amplitudes varying between 1 to 100μA were delivered to the two central electrodes, randomised, separated by 10-20s of dead-time. Each pulse was biphasic, being either anodal first, or cathodal first. Each phase lasted for 50μS with the inter-phase interval being 53μS. Therefore, each stimulation pulse lasted for ~0.1995s. Following certain other stimulation protocols, a post-stimulation spontaneous phase of 15-20 mins was again recorded.

Transition to anaesthesia from wakefulness was achieved first by sedating the animal using a combination of Ketamine 1000 (3 mg/kg intramuscular) and Dexmedetomidine (15 μg/kg intramuscular). The animal was then released from head-fixation and carefully extracted from the experimental chair. The chair was then removed and a custom-built experimental bed was inserted and fixed. This bed was covered with a blanket and an inflatable heating pad was inserted. An injection of Antisedan (75 μg/kg intramuscular) was then given, as an antagonist of the sedative effect of Dexmedetomidine. In one experiment, the animal was laid in a prone position inside a stereotactic frame, while in the rest of the sessions, the animal was laid on its side. Next, the animal was intubated and an IV line was laid. Inhalation anaesthesia was initiated using 2% of Sevoflurane. The ventilator was switched on, and on confirmation of stable vitals, the door of the faraday cage was closed. After ~80-90 minutes from the first injection, the LS experimental epoch was started by changing to and maintaining the anaesthesia at a low level of 1-1.5%. In one session, a paralytic agent, namely Curare, was used. After the end of the LS epoch, the inhalant anaesthesia was increased to 3% (DS). Crucially, we continued to record during this entire process thereby making sure that we were monitoring the same population of neurons throughout the 4 experimental phases.

At the end of the DS epoch, the inhalant anaesthesia was gradually reduced to 0. Upon awakening, the monkey was extubated, the IV line and rectal thermometer was removed, and disconnected from the ventilator and vitals monitor. Next, the animal was placed in the recovery box and returned to its cage. Finally, the animal was monitored for full recovery for the next 24 hours.

Corresponding authors ADwarakanath@dpz.eu; fpanag@psych.uoa.gr

Evaluation of resting state activity

To statistically characterise the effects of the levels of anaesthesia, we fit a 2-state Hidden Markov Model (HMM) to the data. A firing rate threshold of 0.05 spikes/s (Monkey 1) or 2.5 spikes/s (Monkey 2) was set to exclude non-firing channels in the resting state periods, after which spikes were binned in 25ms (Monkey 2) or 50ms (Monkey 1) bins, and then summed and normalised to obtain the population firing vector. To this population vector for each state, k-means clustering was applied to obtain 2 distinct firing rate regimes. These cluster-centres were normalised and used as the initial emission probabilities ($p(EM_{init})$). Initial transition probabilities ($p(TR_{init})$) were drawn from a positive-normal distribution. An initial state sequence guess was obtained by setting all data above the mean to 2, and those below to 1. The HMM was trained on this data to obtain the learned $p(EM_{final})$ and $p(TR_{final})$. These learned probabilities were then used to generate the learned state sequence using the Viterbi algorithm, from which the durations of the UP and DOWN states were finally computed. This training and testing were performed using the HMM toolbox in MATLAB.

State time-frequency information was computed via a continuous wavelet transform using a generalised morse wavelet with 7 cycles and a time-bandwidth product of 3 x 30 at a sampling rate of 500Hz.

Corresponding authors ADwarakanath@dpz.eu; fpanag@psych.uoa.gr

We start with a time-domain signal $x(t)$, i.e. the LFP during QW, LS or DS, and a wavelet $\psi(t)$ with a centre-frequency ω, of Pth order (corresponding to number of cycles), and with γ being the parameter that controls symmetry and thus the time-bandwidth product.

$$\psi_{P,\gamma}(\omega) = \Theta(\omega) a_{P,\gamma} \omega^{\frac{P^2}{\gamma}} \exp\left(-\omega^{\gamma}\right) \tag{1}$$

The continuous wavelet transform (CWT) of the signal is computed using this generalised Morse wavelet as follows -

$$W(t,s) = \frac{1}{\sqrt{s}} \int x(t')\psi^*\left(\frac{t'-t}{s}\right) dt' \tag{2}$$

where s is the scale parameter, and ψ^* is the complex conjugate of the wavelet.

The scalogram is then computed by squaring the absolute value of the CWT.

$$S(t,s) = |W(t,s)|^2 \tag{3}$$

The scalogram is then normalised on the frequency axis to obtain the z-scored scalogram.

$$Z(t,s) = \frac{S(t,s) - \mu_s}{\sigma_s} \tag{4}$$

where μ_s and σ_s are the mean and standard deviation of $S(t,s)$ over the frequency axis, respectively.

Finally, the z-scored CWTs are averaged across valid channels.

$$\bar{Z}(t,s) = \frac{1}{N} \sum_{n=1}^{N} Z_n(t,s) \tag{5}$$

where N is the number of valid channels.

The measure of synchrony (Synchrony Index) was estimated as the sum of the positive-lag auto-correlation function (computed to a 0.5s lag) divided by the number of lags, after which it was subtracted from 1. We consider only the positive lags after 0, therefore we subtract the mean auto-correlation from the peak-value (i.e. 1 at lag-0 when the ACF is normalised).

For a discrete signal of finite length $x(t)$, the synchrony index (SI) is calculated as -

$$SI = 1 - \frac{1}{N}\sum_{\tau=0}^{N} R_n(\tau) \tag{1}$$

where $R_n(\tau)$ is the autocorrelation function computed as -

$$R(\tau) = \frac{1}{T}\sum_{i=1}^{T-\tau} x(i)x(i+\tau) \tag{2}$$

which is then normalised by the zero-lag coefficient, as -

$$R_n(\tau) = \frac{R(\tau)}{R(0)} = \frac{\sum_{i=1}^{T-\tau} x(i)x(i+\tau)}{\sum_{i=1}^{T} x(i)^2} \tag{3}$$

Computing stimulation-related measures

To obtain the onset of each stimulation, the recorded pulse onset-offset analogue signal was differentiated, and zero crossings were detected. These onsets and offsets were sorted into their respective amplitude trials using the trial structure log file corresponding to each epoch. LFPs and spikes were collected for each trial and channel, and aligned to the stimulation offset. Resting state epochs were segmented from the recording using their respective epoch tags.

Mean responses to each stimulation amplitude were computed by concatenating the channel and trial LFPs and PSTHs and then averaging them. The errors were thus the standard deviation across these collapsed samples normalised by the square root of the number of channels, and finally multiplied by 1.96 to obtain the 95% CI.

Response characteristics of the neuronal discharge patterns, namely the first transient and subsequent rebound(s), and the LFP response, were characterised using MATLAB's in-built *findpeaks* function. The dispersal was calculated as the distance to

the cluster centre(s), which roughly corresponds to the variance of a normal distribution. For multi-peak rebound, k-means with n clusters was run to fit the underlying normal distributions.

LFP and spiking response characteristics comparisons were performed pairwise across state combinations (QW vs LS, QW vs DS, LS vs DS), using bootstrapped resampling. The differences were evaluated as the 95% confidence intervals (CI) on 10000 resampling runs.

LFP modulation -

$$SE^n_{\text{pre}} = \frac{1}{t}\sqrt{\sum_{k=1}^{K}(\text{x(t)}^k_{\text{pre}})^2}, \quad SE^k_{\text{post}} = \frac{1}{t}\sqrt{\sum_{k=1}^{K}(\text{x(t)}^k_{\text{post}})^2}$$

$$SE^n = \frac{SE^n_{\text{post}} - SE^n_{\text{pre}}}{SE^n_{\text{post}} + SE^n_{\text{pre}}} \times 100$$

$$SE^n_{\text{pre}} = \sqrt{\sum_{k=1}^{K}(\text{x(t)}^k_{\text{pre}})^2}, \quad SE^k_{\text{post}} = \sqrt{\sum_{k=1}^{K}(\text{x(t)}^k_{\text{post}})^2}$$

$$SE^n = \frac{SE^n_{\text{post}} - SE^n_{\text{pre}}}{SE^n_{\text{post}} + SE^n_{\text{pre}}} \times 100$$

where x(t) represents the LFP signal, k represents the trial index, and n represents the channel index.

The existence and strength of non-monotonicity in the spatial spread of field activity modulation was evaluated using a Bayesian bootstrap on 4 hypotheses, viz.

flat, increasing, decreasing, and non-monotonic. Because the distances increase in even number pitch increments, the data and function were divided into “nearby” and “ far away” populations. The sum of the first differential was computed on these chunks. A 0 or positive index indicates non-monotonicity, whereas the magnitude of the negative sum denotes the steepness of the monotonic decrease. After 10000 bootstrapping runs, the hypothesis with the highest probability (above 0.25) was chosen as the most probable curve shape.

The MATLAB statistics and machine learning toolbox was used to implement all statistical analyses, with custom-written scripts.

References

1. Koch, C., Massimini, M., Boly, M., and Tononi, G. (2016). Neural correlates of consciousness: progress and problems. Nat. Rev. Neurosci. *17*, 307–321. 10.1038/nrn.2016.22.

2. Boly, M., Massimini, M., Tsuchiya, N., Postle, B.R., Koch, C., and Tononi, G. (2017). Are the neural correlates of consciousness in the front or in the back of the cerebral cortex? clinical and neuroimaging evidence. J. Neurosci. *37*, 9603–9613. 10.1523/JNEUROSCI.3218-16.2017.

3. Laureys, S. (2005). The neural correlate of (un)awareness: lessons from the vegetative state. Trends Cogn Sci (Regul Ed) *9*, 556–559. 10.1016/j.tics.2005.10.010.

4. Boly, M., Seth, A.K., Wilke, M., Ingmundson, P., Baars, B., Laureys, S., Edelman, D.B., and Tsuchiya, N. (2013). Consciousness in humans and non-human animals: recent advances and future directions. Front. Psychol. *4*, 625. 10.3389/fpsyg.2013.00625.

5. Edlow, B.L., Claassen, J., Schiff, N.D., and Greer, D.M. (2021). Recovery from disorders of consciousness: mechanisms, prognosis and emerging therapies. Nat. Rev. Neurol. *17*, 135–156. 10.1038/s41582-020-00428-x.

6. Gosseries, O., Di, H., Laureys, S., and Boly, M. (2014). Measuring consciousness in severely damaged brains. Annu. Rev. Neurosci. *37*, 457–478. 10.1146/annurev-neuro-062012-170339.

7. Giacino, J.T., Fins, J.J., Laureys, S., and Schiff, N.D. (2014). Disorders of consciousness after acquired brain injury: the state of the science. Nat. Rev. Neurol. *10*, 99–114. 10.1038/nrneurol.2013.279.

Corresponding authors ADwarakanath@dpz.eu; fpanag@psych.uoa.gr

8. Seth, A.K., and Bayne, T. (2022). Theories of consciousness. Nat. Rev. Neurosci. *23*, 439–452. 10.1038/s41583-022-00587-4.

9. Signorelli, C.M., Szczotka, J., and Prentner, R. (2021). Explanatory profiles of models of consciousness - towards a systematic classification. Neurosci. Conscious. *2021*, niab021. 10.1093/nc/niab021.

10. Pal, D., Dean, J.G., Liu, T., Li, D., Watson, C.J., Hudetz, A.G., and Mashour, G.A. (2018). Differential role of prefrontal and parietal cortices in controlling level of consciousness. Curr. Biol. *28*, 2145-2152.e5. 10.1016/j.cub.2018.05.025.

11. Odegaard, B., Knight, R.T., and Lau, H. (2017). Should a few null findings falsify prefrontal theories of conscious perception? J. Neurosci. *37*, 9593–9602. 10.1523/JNEUROSCI.3217-16.2017.

12. Michel, M., and Morales, J. (2019). Minority reports: Consciousness and the prefrontal cortex. Mind & Language. 10.1111/mila.12264.

13. Bartels, A. (2021). Consciousness: What is the role of prefrontal cortex? Curr. Biol. *31*, R853–R856. 10.1016/j.cub.2021.05.012.

14. Bor, D., and Seth, A.K. (2012). Consciousness and the prefrontal parietal network: insights from attention, working memory, and chunking. Front. Psychol. *3*, 63. 10.3389/fpsyg.2012.00063.

15. Dehaene, S., and Changeux, J.-P. (2011). Experimental and theoretical approaches to conscious processing. Neuron *70*, 200–227. 10.1016/j.neuron.2011.03.018.

16. Mashour, G.A., Roelfsema, P., Changeux, J.-P., and Dehaene, S. (2020). Conscious processing and the global neuronal workspace hypothesis. Neuron *105*, 776–798. 10.1016/j.neuron.2020.01.026.

17. Dehaene, S., and Naccache, L. (2001). Towards a cognitive neuroscience of consciousness: basic evidence and a workspace framework. Cognition *79*, 1–37. 10.1016/S0010-0277(00)00123-2.

18. Dehaene, S., Kerszberg, M., and Changeux, J.P. (1998). A neuronal model of a global workspace in effortful cognitive tasks. Proc Natl Acad Sci USA *95*, 14529–14534. 10.1073/pnas.95.24.14529.

19. Knapen, T., Brascamp, J., Pearson, J., van Ee, R., and Blake, R. (2011). The role of frontal and parietal brain areas in bistable perception. J. Neurosci. *31*, 10293–10301. 10.1523/JNEUROSCI.1727-11.2011.

20. Sterzer, P., Kleinschmidt, A., and Rees, G. (2009). The neural bases of multistable perception. Trends Cogn Sci (Regul Ed) *13*, 310–318. 10.1016/j.tics.2009.04.006.

Corresponding authors ADwarakanath@dpz.eu; fpanag@psych.uoa.gr

21. Weilnhammer, V.A., Ludwig, K., Hesselmann, G., and Sterzer, P. (2013). Frontoparietal cortex mediates perceptual transitions in bistable perception. J. Neurosci. *33*, 16009–16015. 10.1523/JNEUROSCI.1418-13.2013.

22. Panagiotaropoulos, T.I., Deco, G., Kapoor, V., and Logothetis, N.K. (2012). Neuronal discharges and gamma oscillations explicitly reflect visual consciousness in the lateral prefrontal cortex. Neuron *74*, 924–935. 10.1016/j.neuron.2012.04.013.

23. Kapoor, V., Dwarakanath, A., Safavi, S., Werner, J., Besserve, M., Panagiotaropoulos, T.I., and Logothetis, N.K. (2022). Decoding internally generated transitions of conscious contents in the prefrontal cortex without subjective reports. Nat. Commun. *13*, 1535. 10.1038/s41467-022-28897-2.

24. Dwarakanath, A., Kapoor, V., Werner, J., Safavi, S., Fedorov, L.A., Logothetis, N.K., and Panagiotaropoulos, T.I. (2023). Bistability of prefrontal states gates access to consciousness. Neuron *111*, 1666-1683.e4. 10.1016/j.neuron.2023.02.027.

25. Bellet, J., Gay, M., Dwarakanath, A., Jarraya, B., van Kerkoerle, T., Dehaene, S., and Panagiotaropoulos, T.I. (2022). Decoding rapidly presented visual stimuli from prefrontal ensembles without report nor post-perceptual processing. Neurosci. Conscious. *2022*, niac005. 10.1093/nc/niac005.

26. Bellet, M.E., Gay, M., Bellet, J., Jarraya, B., Dehaene, S., van Kerkoerle, T., and Panagiotaropoulos, T.I. (2021). Prefrontal neural ensembles encode an internal model of visual sequences and their violations. BioRxiv. 10.1101/2021.10.04.463064.

27. Petrides, M., and Pandya, D.N. (2009). Distinct parietal and temporal pathways to the homologues of Broca's area in the monkey. PLoS Biol. *7*, e1000170. 10.1371/journal.pbio.1000170.

28. Petrides, M., and Pandya, D.N. (1984). Projections to the frontal cortex from the posterior parietal region in the rhesus monkey. J. Comp. Neurol. *228*, 105–116. 10.1002/cne.902280110.

29. Markov, N.T., Ercsey-Ravasz, M., Van Essen, D.C., Knoblauch, K., Toroczkai, Z., and Kennedy, H. (2013). Cortical high-density counterstream architectures. Science *342*, 1238406. 10.1126/science.1238406.

30. Yeterian, E.H., Pandya, D.N., Tomaiuolo, F., and Petrides, M. (2012). The cortical connectivity of the prefrontal cortex in the monkey brain. Cortex *48*, 58–81. 10.1016/j.cortex.2011.03.004.

31. Raccah, O., Block, N., and Fox, K.C.R. (2021). Does the Prefrontal Cortex Play an Essential Role in Consciousness? Insights from Intracranial Electrical Stimulation of the Human Brain. J. Neurosci. *41*, 2076–2087. 10.1523/JNEUROSCI.1141-20.2020.

Corresponding authors ADwarakanath@dpz.eu; fpanag@psych.uoa.gr

32. Alkire, M.T., Hudetz, A.G., and Tononi, G. (2008). Consciousness and anesthesia. Science *322*, 876–880. 10.1126/science.1149213.

33. Brown, E.N., Lydic, R., and Schiff, N.D. (2010). General anesthesia, sleep, and coma. N. Engl. J. Med. *363*, 2638–2650. 10.1056/NEJMra0808281.

34. MacDonald, A.A., Naci, L., MacDonald, P.A., and Owen, A.M. (2015). Anesthesia and neuroimaging: investigating the neural correlates of unconsciousness. Trends Cogn Sci (Regul Ed) *19*, 100–107. 10.1016/j.tics.2014.12.005.

35. Bonhomme, V., Staquet, C., Montupil, J., Defresne, A., Kirsch, M., Martial, C., Vanhaudenhuyse, A., Chatelle, C., Larroque, S.K., Raimondo, F., et al. (2019). General anesthesia: A probe to explore consciousness. Front. Syst. Neurosci. *13*, 36. 10.3389/fnsys.2019.00036.

36. Purdon, P.L., Pierce, E.T., Mukamel, E.A., Prerau, M.J., Walsh, J.L., Wong, K.F.K., Salazar-Gomez, A.F., Harrell, P.G., Sampson, A.L., Cimenser, A., et al. (2013). Electroencephalogram signatures of loss and recovery of consciousness from propofol. Proc Natl Acad Sci USA *110*, E1142-51. 10.1073/pnas.1221180110.

37. Demertzi, A., Tagliazucchi, E., Dehaene, S., Deco, G., Barttfeld, P., Raimondo, F., Martial, C., Fernández-Espejo, D., Rohaut, B., Voss, H.U., et al. (2019). Human consciousness is supported by dynamic complex patterns of brain signal coordination. Sci. Adv. *5*, eaat7603. 10.1126/sciadv.aat7603.

38. Tinker, J.H., Sharbrough, F.W., and Michenfelder, J.D. (1977). Anterior shift of the dominant EEG rhytham during anesthesia in the Java monkey: correlation with anesthetic potency. Anesthesiology *46*, 252–259. 10.1097/00000542-197704000-00005.

39. Vijayan, S., Ching, S., Purdon, P.L., Brown, E.N., and Kopell, N.J. (2013). Thalamocortical mechanisms for the anteriorization of α rhythms during propofol-induced unconsciousness. J. Neurosci. *33*, 11070–11075. 10.1523/JNEUROSCI.5670-12.2013.

40. Bastos, A.M., Donoghue, J.A., Brincat, S.L., Mahnke, M., Yanar, J., Correa, J., Waite, A.S., Lundqvist, M., Roy, J., Brown, E.N., et al. (2021). Neural effects of propofol-induced unconsciousness and its reversal using thalamic stimulation. eLife *10*. 10.7554/eLife.60824.

41. Vincent, J.L., Patel, G.H., Fox, M.D., Snyder, A.Z., Baker, J.T., Van Essen, D.C., Zempel, J.M., Snyder, L.H., Corbetta, M., and Raichle, M.E. (2007). Intrinsic functional architecture in the anaesthetized monkey brain. Nature *447*, 83–86. 10.1038/nature05758.

42. Schrouff, J., Perlbarg, V., Boly, M., Marrelec, G., Boveroux, P., Vanhaudenhuyse, A., Bruno, M.-A., Laureys, S., Phillips, C., Pélégrini-Issac, M., et al. (2011). Brain

functional integration decreases during propofol-induced loss of consciousness. Neuroimage *57*, 198–205. 10.1016/j.neuroimage.2011.04.020.

43. Akeju, O., Westover, M.B., Pavone, K.J., Sampson, A.L., Hartnack, K.E., Brown, E.N., and Purdon, P.L. (2014). Effects of sevoflurane and propofol on frontal electroencephalogram power and coherence. Anesthesiology *121*, 990–998. 10.1097/ALN.0000000000000436.

44. Akeju, O., and Brown, E.N. (2017). Neural oscillations demonstrate that general anesthesia and sedative states are neurophysiologically distinct from sleep. Curr. Opin. Neurobiol. *44*, 178–185. 10.1016/j.conb.2017.04.011.

45. John, E.R., and Prichep, L.S. (2005). The anesthetic cascade: a theory of how anesthesia suppresses consciousness. Anesthesiology *102*, 447–471. 10.1097/00000542-200502000-00030.

46. Franks, N.P. (2008). General anaesthesia: from molecular targets to neuronal pathways of sleep and arousal. Nat. Rev. Neurosci. *9*, 370–386. 10.1038/nrn2372.

47. Steriade, M., Nuñez, A., and Amzica, F. (1993). A novel slow (< 1 Hz) oscillation of neocortical neurons in vivo: depolarizing and hyperpolarizing components. J. Neurosci. *13*, 3252–3265. 10.1523/JNEUROSCI.13-08-03252.1993.

48. Uhrig, L., Dehaene, S., and Jarraya, B. (2014). Cerebral mechanisms of general anesthesia. Ann Fr Anesth Reanim *33*, 72–82. 10.1016/j.annfar.2013.11.005.

49. Lee, U., Ku, S., Noh, G., Baek, S., Choi, B., and Mashour, G.A. (2013). Disruption of frontal-parietal communication by ketamine, propofol, and sevoflurane. Anesthesiology *118*, 1264–1275. 10.1097/ALN.0b013e31829103f5.

50. Hudetz, A.G., and Mashour, G.A. (2016). Disconnecting consciousness: is there a common anesthetic end point? Anesth. Analg. *123*, 1228–1240. 10.1213/ANE.0000000000001353.

51. Sellers, K.K., Bennett, D.V., Hutt, A., Williams, J.H., and Fröhlich, F. (2015). Awake vs. anesthetized: layer-specific sensory processing in visual cortex and functional connectivity between cortical areas. J. Neurophysiol. *113*, 3798–3815. 10.1152/jn.00923.2014.

52. Sarasso, S., Boly, M., Napolitani, M., Gosseries, O., Charland-Verville, V., Casarotto, S., Rosanova, M., Casali, A.G., Brichant, J.-F., Boveroux, P., et al. (2015). Consciousness and Complexity during Unresponsiveness Induced by Propofol, Xenon, and Ketamine. Curr. Biol. *25*, 3099–3105. 10.1016/j.cub.2015.10.014.

53. Deco, G., Jirsa, V.K., Robinson, P.A., Breakspear, M., and Friston, K. (2008). The dynamic brain: from spiking neurons to neural masses and cortical fields. PLoS Comput. Biol. *4*, e1000092. 10.1371/journal.pcbi.1000092.

Corresponding authors ADwarakanath@dpz.eu; fpanag@psych.uoa.gr

54. Bettinardi, R.G., Tort-Colet, N., Ruiz-Mejias, M., Sanchez-Vives, M.V., and Deco, G. (2015). Gradual emergence of spontaneous correlated brain activity during fading of general anesthesia in rats: Evidences from fMRI and local field potentials. Neuroimage *114*, 185–198. 10.1016/j.neuroimage.2015.03.037.

55. Casali, A.G., Gosseries, O., Rosanova, M., Boly, M., Sarasso, S., Casali, K.R., Casarotto, S., Bruno, M.-A., Laureys, S., Tononi, G., et al. (2013). A theoretically based index of consciousness independent of sensory processing and behavior. Sci. Transl. Med. *5*, 198ra105. 10.1126/scitranslmed.3006294.

56. Sarasso, S., Rosanova, M., Casali, A.G., Casarotto, S., Fecchio, M., Boly, M., Gosseries, O., Tononi, G., Laureys, S., and Massimini, M. (2014). Quantifying cortical EEG responses to TMS in (un)consciousness. Clin. EEG Neurosci. *45*, 40–49. 10.1177/1550059413513723.

57. Fetsch, C.R., Kiani, R., Newsome, W.T., and Shadlen, M.N. (2014). Effects of cortical microstimulation on confidence in a perceptual decision. Neuron *83*, 797–804. 10.1016/j.neuron.2014.07.011.

58. Chen, X., Wang, F., Fernandez, E., and Roelfsema, P.R. (2020). Shape perception via a high-channel-count neuroprosthesis in monkey visual cortex. Science *370*, 1191–1196. 10.1126/science.abd7435.

59. van Vugt, B., Dagnino, B., Vartak, D., Safaai, H., Panzeri, S., Dehaene, S., and Roelfsema, P.R. (2018). The threshold for conscious report: Signal loss and response bias in visual and frontal cortex. Science *360*, 537–542. 10.1126/science.aar7186.

60. Hanks, T.D., Ditterich, J., and Shadlen, M.N. (2006). Microstimulation of macaque area LIP affects decision-making in a motion discrimination task. Nat. Neurosci. *9*, 682–689. 10.1038/nn1683.

61. Stephen, E.P., Hotan, G.C., Pierce, E.T., Harrell, P.G., Walsh, J.L., Brown, E.N., and Purdon, P.L. (2020). Broadband slow-wave modulation in posterior and anterior cortex tracks distinct states of propofol-induced unconsciousness. Sci. Rep. *10*, 13701. 10.1038/s41598-020-68756-y.

62. Kroeger, D., and Amzica, F. (2007). Hypersensitivity of the anesthesia-induced comatose brain. J. Neurosci. *27*, 10597–10607. 10.1523/JNEUROSCI.3440-07.2007.

63. Ferron, J.-F., Kroeger, D., Chever, O., and Amzica, F. (2009). Cortical inhibition during burst suppression induced with isoflurane anesthesia. J. Neurosci. *29*, 9850–9860. 10.1523/JNEUROSCI.5176-08.2009.

64. Petrides, M., Tomaiuolo, F., Yeterian, E.H., and Pandya, D.N. (2012). The prefrontal cortex: comparative architectonic organization in the human and the macaque monkey brains. Cortex *48*, 46–57. 10.1016/j.cortex.2011.07.002.

Corresponding authors ADwarakanath@dpz.eu; fpanag@psych.uoa.gr

65. Kritzer, M.F., and Goldman-Rakic, P.S. (1995). Intrinsic circuit organization of the major layers and sublayers of the dorsolateral prefrontal cortex in the rhesus monkey. J. Comp. Neurol. *359*, 131–143. 10.1002/cne.903590109.

66. Petrides, M. (2005). Lateral prefrontal cortex: architectonic and functional organization. Philos. Trans. R. Soc. Lond. B Biol. Sci. *360*, 781–795. 10.1098/rstb.2005.1631.

67. Rigotti, M., Barak, O., Warden, M.R., Wang, X.-J., Daw, N.D., Miller, E.K., and Fusi, S. (2013). The importance of mixed selectivity in complex cognitive tasks. Nature *497*, 585–590. 10.1038/nature12160.

68. Mante, V., Sussillo, D., Shenoy, K.V., and Newsome, W.T. (2013). Context-dependent computation by recurrent dynamics in prefrontal cortex. Nature *503*, 78–84. 10.1038/nature12742.

69. Miller, E.K., and Cohen, J.D. (2001). An integrative theory of prefrontal cortex function. Annu. Rev. Neurosci. *24*, 167–202. 10.1146/annurev.neuro.24.1.167.

70. Miller, E.K., Lundqvist, M., and Bastos, A.M. (2018). Working Memory 2.0. Neuron *100*, 463–475. 10.1016/j.neuron.2018.09.023.

71. Friedman, N.P., and Robbins, T.W. (2022). The role of prefrontal cortex in cognitive control and executive function. Neuropsychopharmacology *47*, 72–89. 10.1038/s41386-021-01132-0.

72. Stuss, D.T. (2011). Functions of the frontal lobes: relation to executive functions. J. Int. Neuropsychol. Soc. *17*, 759–765. 10.1017/S1355617711000695.

73. Munakata, Y., Herd, S.A., Chatham, C.H., Depue, B.E., Banich, M.T., and O'Reilly, R.C. (2011). A unified framework for inhibitory control. Trends Cogn Sci (Regul Ed) *15*, 453–459. 10.1016/j.tics.2011.07.011.

74. Jercog, D., Roxin, A., Barthó, P., Luczak, A., Compte, A., and de la Rocha, J. (2017). UP-DOWN cortical dynamics reflect state transitions in a bistable network. eLife *6*. 10.7554/eLife.22425.

75. Torao-Angosto, M., Manasanch, A., Mattia, M., and Sanchez-Vives, M.V. (2021). Up and Down States During Slow Oscillations in Slow-Wave Sleep and Different Levels of Anesthesia. Front. Syst. Neurosci. *15*, 609645. 10.3389/fnsys.2021.609645.

76. Norton, L., Hutchison, R.M., Young, G.B., Lee, D.H., Sharpe, M.D., and Mirsattari, S.M. (2012). Disruptions of functional connectivity in the default mode network of comatose patients. Neurology *78*, 175–181. 10.1212/WNL.0b013e31823fcd61.

77. Lee, U., Kim, S., Noh, G.-J., Choi, B.-M., Hwang, E., and Mashour, G.A. (2009). The directionality and functional organization of frontoparietal connectivity during

consciousness and anesthesia in humans. Conscious. Cogn. *18*, 1069–1078. 10.1016/j.concog.2009.04.004.

78. Bodien, Y.G., Chatelle, C., and Edlow, B.L. (2017). Functional networks in disorders of consciousness. Semin. Neurol. *37*, 485–502. 10.1055/s-0037-1607310.

79. Yang, Y., He, Q., Dang, Y., Xia, X., Xu, X., Chen, X., Zhao, J., and He, J. (2023). Long-term functional outcomes improved with deep brain stimulation in patients with disorders of consciousness. Stroke Vasc. Neurol. *8*, 368–378. 10.1136/svn-2022-001998.

80. Quraishi, I.H., Benjamin, C.F., Spencer, D.D., Blumenfeld, H., and Alkawadri, R. (2017). Impairment of consciousness induced by bilateral electrical stimulation of the frontal convexity. Epilepsy Behav. Case Rep. *8*, 117–122. 10.1016/j.ebcr.2017.09.006.

81. West, T.O., Magill, P.J., Sharott, A., Litvak, V., Farmer, S.F., and Cagnan, H. (2022). Stimulating at the right time to recover network states in a model of the cortico-basal ganglia-thalamic circuit. PLoS Comput. Biol. *18*, e1009887. 10.1371/journal.pcbi.1009887.

82. Koubeissi, M.Z., Bartolomei, F., Beltagy, A., and Picard, F. (2014). Electrical stimulation of a small brain area reversibly disrupts consciousness. Epilepsy Behav. *37*, 32–35. 10.1016/j.yebeh.2014.05.027.

83. Peles, O., Werner-Reiss, U., Bergman, H., Israel, Z., and Vaadia, E. (2020). Phase-Specific Microstimulation Differentially Modulates Beta Oscillations and Affects Behavior. Cell Rep. *30*, 2555-2566.e3. 10.1016/j.celrep.2020.02.005.

84. Salzman, C.D., Britten, K.H., and Newsome, W.T. (1990). Cortical microstimulation influences perceptual judgements of motion direction. Nature *346*, 174–177. 10.1038/346174a0.

85. Houweling, A.R., and Brecht, M. (2008). Behavioural report of single neuron stimulation in somatosensory cortex. Nature *451*, 65–68. 10.1038/nature06447.

86. Logothetis, N.K., Augath, M., Murayama, Y., Rauch, A., Sultan, F., Goense, J., Oeltermann, A., and Merkle, H. (2010). The effects of electrical microstimulation on cortical signal propagation. Nat. Neurosci. *13*, 1283–1291. 10.1038/nn.2631.

87. Tehovnik, E.J., Tolias, A.S., Sultan, F., Slocum, W.M., and Logothetis, N.K. (2006). Direct and indirect activation of cortical neurons by electrical microstimulation. J. Neurophysiol. *96*, 512–521. 10.1152/jn.00126.2006.

88. Afraz, S.-R., Kiani, R., and Esteky, H. (2006). Microstimulation of inferotemporal cortex influences face categorization. Nature *442*, 692–695. 10.1038/nature04982.

89. Caldwell, D.J., Ojemann, J.G., and Rao, R.P.N. (2019). Direct Electrical Stimulation in Electrocorticographic Brain-Computer Interfaces: Enabling Technologies for Input to Cortex. Front. Neurosci. *13*, 804. 10.3389/fnins.2019.00804.

90. de Lafuente, V. (2018). Regaining the senses of touch and movement. eLife *7*. 10.7554/eLife.36137.

91. Flesher, S.N., Collinger, J.L., Foldes, S.T., Weiss, J.M., Downey, J.E., Tyler-Kabara, E.C., Bensmaia, S.J., Schwartz, A.B., Boninger, M.L., and Gaunt, R.A. (2016). Intracortical microstimulation of human somatosensory cortex. Sci. Transl. Med. *8*, 361ra141. 10.1126/scitranslmed.aaf8083.

92. Najarpour Foroushani, A., Pack, C.C., and Sawan, M. (2018). Cortical visual prostheses: from microstimulation to functional percept. J. Neural Eng. *15*, 021005. 10.1088/1741-2552/aaa904.

93. Fox, K.C.R., Yih, J., Raccah, O., Pendekanti, S.L., Limbach, L.E., Maydan, D.D., and Parvizi, J. (2018). Changes in subjective experience elicited by direct stimulation of the human orbitofrontal cortex. Neurology *91*, e1519–e1527. 10.1212/WNL.0000000000006358.

94. Moore, T., and Armstrong, K.M. (2003). Selective gating of visual signals by microstimulation of frontal cortex. Nature *421*, 370–373. 10.1038/nature01341.

95. Torres-Gomez, S., Blonde, J.D., Mendoza-Halliday, D., Kuebler, E., Everest, M., Wang, X.J., Inoue, W., Poulter, M.O., and Martinez-Trujillo, J. (2020). Changes in the Proportion of Inhibitory Interneuron Types from Sensory to Executive Areas of the Primate Neocortex: Implications for the Origins of Working Memory Representations. Cereb. Cortex *30*, 4544–4562. 10.1093/cercor/bhaa056.

96. Tremblay, R., Lee, S., and Rudy, B. (2016). Gabaergic interneurons in the neocortex: from cellular properties to circuits. Neuron *91*, 260–292. 10.1016/j.neuron.2016.06.033.

97. Ferrer, C., and De Marco García, N.V. (2022). The role of inhibitory interneurons in circuit assembly and refinement across sensory cortices. Front. Neural Circuits *16*, 866999. 10.3389/fncir.2022.866999.

98. Wu, Y.K., Miehl, C., and Gjorgjieva, J. (2022). Regulation of circuit organization and function through inhibitory synaptic plasticity. Trends Neurosci. *45*, 884–898. 10.1016/j.tins.2022.10.006.

99. Goyal, N., and Chad, D.A. (2014). Motor Control, Peripheral. In Encyclopedia of the neurological sciences (Elsevier), pp. 100–106. 10.1016/B978-0-12-385157-4.00618-7.

100. Herstel, L.J., and Wierenga, C.J. (2021). Network control through coordinated inhibition. Curr. Opin. Neurobiol. *67*, 34–41. 10.1016/j.conb.2020.08.001.

Corresponding authors ADwarakanath@dpz.eu; fpanag@psych.uoa.gr

101. Swanson, O.K., and Maffei, A. (2019). From hiring to firing: activation of inhibitory neurons and their recruitment in behavior. Front. Mol. Neurosci. *12*, 168. 10.3389/fnmol.2019.00168.

102. Santos, B.A., Gomes, R.M., and Husbands, P. (2021). The role of rebound spikes in the maintenance of self-sustained neural spiking activity. Nonlinear Dyn. *105*, 767–784. 10.1007/s11071-021-06581-2.

103. Terman, D., Ahn, S., Wang, X., and Just, W. (2008). Reducing neuronal networks to discrete dynamics. Physica D *237*, 324–338. 10.1016/j.physd.2007.09.011.

104. Steriade, M., Amzica, F., and Contreras, D. (1994). Cortical and thalamic cellular correlates of electroencephalographic burst-suppression. Electroencephalogr. Clin. Neurophysiol. *90*, 1–16. 10.1016/0013-4694(94)90108-2.

105. Mashour, G.A. (2014). Top-down mechanisms of anesthetic-induced unconsciousness. Front. Syst. Neurosci. *8*, 115. 10.3389/fnsys.2014.00115.

106. Hao, X., Ou, M., Zhang, D., Zhao, W., Yang, Y., Liu, J., Yang, H., Zhu, T., Li, Y., and Zhou, C. (2020). The effects of general anesthetics on synaptic transmission. Curr. Neuropharmacol. *18*, 936–965. 10.2174/1570159X18666200227125854.

107. Antkowiak, B. (1999). Different actions of general anesthetics on the firing patterns of neocortical neurons mediated by the GABA(A) receptor. Anesthesiology *91*, 500–511. 10.1097/00000542-199908000-00025.

108. Ferrarelli, F., Massimini, M., Sarasso, S., Casali, A., Riedner, B.A., Angelini, G., Tononi, G., and Pearce, R.A. (2010). Breakdown in cortical effective connectivity during midazolam-induced loss of consciousness. Proc Natl Acad Sci USA *107*, 2681–2686. 10.1073/pnas.0913008107.

109. Arnulfo, G., Wang, S.H., Myrov, V., Toselli, B., Hirvonen, J., Fato, M.M., Nobili, L., Cardinale, F., Rubino, A., Zhigalov, A., et al. (2020). Long-range phase synchronization of high-frequency oscillations in human cortex. Nat. Commun. *11*, 5363. 10.1038/s41467-020-18975-8.

110. Poulet, J.F.A., and Crochet, S. (2018). The cortical states of wakefulness. Front. Syst. Neurosci. *12*, 64. 10.3389/fnsys.2018.00064.

111. Harris, A.Z., and Gordon, J.A. (2015). Long-range neural synchrony in behavior. Annu. Rev. Neurosci. *38*, 171–194. 10.1146/annurev-neuro-071714-034111.

112. Greicius, M.D., Kiviniemi, V., Tervonen, O., Vainionpää, V., Alahuhta, S., Reiss, A.L., and Menon, V. (2008). Persistent default-mode network connectivity during light sedation. Hum. Brain Mapp. *29*, 839–847. 10.1002/hbm.20537.

113. Shepherd, G.M., and Grillner, S. eds. (2017). Handbook of brain microcircuits (Oxford University Press) 10.1093/med/9780190636111.001.0001.

114. Rao, S.G., Williams, G.V., and Goldman-Rakic, P.S. (1999). Isodirectional tuning of adjacent interneurons and pyramidal cells during working memory: evidence for microcolumnar organization in PFC. J. Neurophysiol. *81*, 1903–1916. 10.1152/jn.1999.81.4.1903.

115. Constantinidis, C., Williams, G.V., and Goldman-Rakic, P.S. (2002). A role for inhibition in shaping the temporal flow of information in prefrontal cortex. Nat. Neurosci. *5*, 175–180. 10.1038/nn799.

116. Schwartz, M.L., Zheng, D.S., and Goldman-Rakic, P.S. (1988). Periodicity of GABA-containing cells in primate prefrontal cortex. J. Neurosci. *8*, 1962–1970.

117. Lee, A.T., Gee, S.M., Vogt, D., Patel, T., Rubenstein, J.L., and Sohal, V.S. (2014). Pyramidal neurons in prefrontal cortex receive subtype-specific forms of excitation and inhibition. Neuron *81*, 61–68. 10.1016/j.neuron.2013.10.031.

118. Baker, A., Kalmbach, B., Morishima, M., Kim, J., Juavinett, A., Li, N., and Dembrow, N. (2018). Specialized Subpopulations of Deep-Layer Pyramidal Neurons in the Neocortex: Bridging Cellular Properties to Functional Consequences. J. Neurosci. *38*, 5441–5455. 10.1523/JNEUROSCI.0150-18.2018.

119. Murayama, M., and Larkum, M.E. (2009). Enhanced dendritic activity in awake rats. Proc Natl Acad Sci USA *106*, 20482–20486. 10.1073/pnas.0910379106.

120. Gaillard, R., and Del Cul, A. (2007). [A scientific model of consciousness: implications for neuropsychiatic diseases]. Psychol. Neuropsychiatr. Vieil. *5*, 261–267.

121. Kapoor, V., Besserve, M., Logothetis, N.K., and Panagiotaropoulos, T.I. (2018). Parallel and functionally segregated processing of task phase and conscious content in the prefrontal cortex. Commun. Biol. *1*, 215. 10.1038/s42003-018-0225-1.

122. Constantinidis, C., and Qi, X.-L. (2018). Representation of spatial and feature information in the monkey dorsal and ventral prefrontal cortex. Front. Integr. Neurosci. *12*, 31. 10.3389/fnint.2018.00031.

123. Afrasiabi, M., Redinbaugh, M.J., Phillips, J.M., Kambi, N.A., Mohanta, S., Raz, A., Haun, A.M., and Saalmann, Y.B. (2021). Consciousness depends on integration between parietal cortex, striatum, and thalamus. Cell Syst. *12*, 363-373.e11. 10.1016/j.cels.2021.02.003.

124. Zhao, T., Zhu, Y., Tang, H., Xie, R., Zhu, J., and Zhang, J.H. (2019). Consciousness: new concepts and neural networks. Front. Cell. Neurosci. *13*, 302. 10.3389/fncel.2019.00302.

125. Franke, F., Fiscella, M., Sevelev, M., Roska, B., Hierlemann, A., and da Silveira, R.A. (2016). Structures of neural correlation and how they favor coding. Neuron *89*, 409–422. 10.1016/j.neuron.2015.12.037.

126. Stevenson, I.H., London, B.M., Oby, E.R., Sachs, N.A., Reimer, J., Englitz, B., David, S.V., Shamma, S.A., Blanche, T.J., Mizuseki, K., et al. (2012). Functional connectivity and tuning curves in populations of simultaneously recorded neurons. PLoS Comput. Biol. *8*, e1002775. 10.1371/journal.pcbi.1002775.

127. Safavi, S., Dwarakanath, A., Kapoor, V., Werner, J., Hatsopoulos, N.G., Logothetis, N.K., and Panagiotaropoulos, T.I. (2018). Nonmonotonic spatial structure of interneuronal correlations in prefrontal microcircuits. Proc Natl Acad Sci USA *115*, E3539–E3548. 10.1073/pnas.1802356115.

128. Rosenbaum, R., Smith, M.A., Kohn, A., Rubin, J.E., and Doiron, B. (2017). The spatial structure of correlated neuronal variability. Nat. Neurosci. *20*, 107–114. 10.1038/nn.4433.

129. Wang, Y., Markram, H., Goodman, P.H., Berger, T.K., Ma, J., and Goldman-Rakic, P.S. (2006). Heterogeneity in the pyramidal network of the medial prefrontal cortex. Nat. Neurosci. *9*, 534–542. 10.1038/nn1670.

130. Sugihara, T., Diltz, M.D., Averbeck, B.B., and Romanski, L.M. (2006). Integration of auditory and visual communication information in the primate ventrolateral prefrontal cortex. J. Neurosci. *26*, 11138–11147. 10.1523/JNEUROSCI.3550-06.2006.

131. O'Reilly, R.C. (2010). The What and How of prefrontal cortical organization. Trends Neurosci. *33*, 355–361. 10.1016/j.tins.2010.05.002.

132. Pipa, G., and Munk, M.H.J. (2011). Higher Order Spike Synchrony in Prefrontal Cortex during Visual Memory. Front. Comput. Neurosci. *5*, 23. 10.3389/fncom.2011.00023.

133. Ramani, R., and Wardhan, R. (2008). Understanding anesthesia through functional imaging. Curr. Opin. Anaesthesiol. *21*, 530–536. 10.1097/ACO.0b013e32830edbf3.

134. Ramani, R., Qiu, M., and Constable, R.T. (2007). Sevoflurane 0.25 MAC preferentially affects higher order association areas: a functional magnetic resonance imaging study in volunteers. Anesth. Analg. *105*, 648–655. 10.1213/01.ane.0000277496.12747.29.

135. Vizuete, J.A., Pillay, S., Diba, K., Ropella, K.M., and Hudetz, A.G. (2012). Monosynaptic functional connectivity in cerebral cortex during wakefulness and under graded levels of anesthesia. Front. Integr. Neurosci. *6*, 90. 10.3389/fnint.2012.00090.

136. Mashour, G.A. (2006). Integrating the science of consciousness and anesthesia. Anesth. Analg. *103*, 975–982. 10.1213/01.ane.0000232442.69757.4a.

Corresponding authors ADwarakanath@dpz.eu; fpanag@psych.uoa.gr

137. Treccani, B. (2018). The neuropsychology of feature binding and conscious perception. Front. Psychol. *9*, 2606. 10.3389/fpsyg.2018.02606.

138. Treisman, A. (2003). Consciousness and perceptual binding. In The unity of consciousnessbinding, integration, and dissociation (Oxford University Press), pp. 95–113. 10.1093/acprof:oso/9780198508571.003.0005.

139. Huang, L. (2010). Characterizing the nature of visual conscious access: the distinction between features and locations. J. Vis. *10*, 24. 10.1167/10.10.24.

140. Pennartz, C.M.A. (2015). Neural mechanisms for conscious representations. In The brain's representational power: on consciousness and the integration of modalities (The MIT Press), pp. 233–264. 10.7551/mitpress/9780262029315.003.0009.

141. Parto Dezfouli, M., Schwedhelm, P., Wibral, M., Treue, S., Daliri, M.R., and Esghaei, M. (2021). A neural correlate of visual feature binding in primate lateral prefrontal cortex. Neuroimage *229*, 117757. 10.1016/j.neuroimage.2021.117757.

142. Bocincova, A., Buschman, T.J., Stokes, M.G., and Manohar, S.G. (2022). Neural signature of flexible coding in prefrontal cortex. Proc Natl Acad Sci USA *119*, e2200400119. 10.1073/pnas.2200400119.

143. Isbister, J.B., Eguchi, A., Ahmad, N., Galeazzi, J.M., Buckley, M.J., and Stringer, S. (2018). A new approach to solving the feature-binding problem in primate vision. Interface Focus *8*, 20180021. 10.1098/rsfs.2018.0021.

144. Martín-Signes, M., Paz-Alonso, P.M., and Chica, A.B. (2019). Connectivity of frontoparietal regions reveals executive attention and consciousness interactions. Cereb. Cortex *29*, 4539–4550. 10.1093/cercor/bhy332.

145. Tasserie, J., Uhrig, L., Sitt, J.D., Manasova, D., Dupont, M., Dehaene, S., and Jarraya, B. (2022). Deep brain stimulation of the thalamus restores signatures of consciousness in a nonhuman primate model. Sci. Adv. *8*, eabl5547. 10.1126/sciadv.abl5547.

146. Pirot, S., Glowinski, J., and Thierry, A.M. (1995). Excitatory responses evoked in prefrontal cortex by mediodorsal thalamic nucleus stimulation: influence of anaesthesia. Eur. J. Pharmacol. *285*, 45–54. 10.1016/0014-2999(95)00377-w.

147. Cruikshank, S.J., Ahmed, O.J., Stevens, T.R., Patrick, S.L., Gonzalez, A.N., Elmaleh, M., and Connors, B.W. (2012). Thalamic control of layer 1 circuits in prefrontal cortex. J. Neurosci. *32*, 17813–17823. 10.1523/JNEUROSCI.3231-12.2012.

148. Bekinschtein, T.A., Dehaene, S., Rohaut, B., Tadel, F., Cohen, L., and Naccache, L. (2009). Neural signature of the conscious processing of auditory regularities. Proc Natl Acad Sci USA *106*, 1672–1677. 10.1073/pnas.0809667106.

Corresponding authors ADwarakanath@dpz.eu; fpanag@psych.uoa.gr

149. Sombeck, J.T., Heye, J., Kumaravelu, K., Goetz, S.M., Peterchev, A.V., Grill, W.M., Bensmaia, S., and Miller, L.E. (2022). Characterizing the short-latency evoked response to intracortical microstimulation across a multi-electrode array. J. Neural Eng. *19*. 10.1088/1741-2552/ac63e8.

150. Callier, T., Brantly, N.W., Caravelli, A., and Bensmaia, S.J. (2020). The frequency of cortical microstimulation shapes artificial touch. Proc Natl Acad Sci USA *117*, 1191–1200. 10.1073/pnas.1916453117.

151. Romo, R., Hernández, A., Zainos, A., and Salinas, E. (1998). Somatosensory discrimination based on cortical microstimulation. Nature *392*, 387–390. 10.1038/32891.

152. Klink, P.C., Dagnino, B., Gariel-Mathis, M.-A., and Roelfsema, P.R. (2017). Distinct feedforward and feedback effects of microstimulation in visual cortex reveal neural mechanisms of texture segregation. Neuron *95*, 209-220.e3. 10.1016/j.neuron.2017.05.033.

153. Voigt, M.B., Hubka, P., and Kral, A. (2017). Intracortical microstimulation differentially activates cortical layers based on stimulation depth. Brain Stimulat. *10*, 684–694. 10.1016/j.brs.2017.02.009.

154. Maynard, E.M., Nordhausen, C.T., and Normann, R.A. (1997). The Utah intracortical Electrode Array: a recording structure for potential brain-computer interfaces. Electroencephalogr. Clin. Neurophysiol. *102*, 228–239. 10.1016/S0013-4694(96)95176-0.

155. Quiroga, R.Q., Nadasdy, Z., and Ben-Shaul, Y. (2004). Unsupervised spike detection and sorting with wavelets and superparamagnetic clustering. Neural Comput. *16*, 1661–1687. 10.1162/089976604774201631.

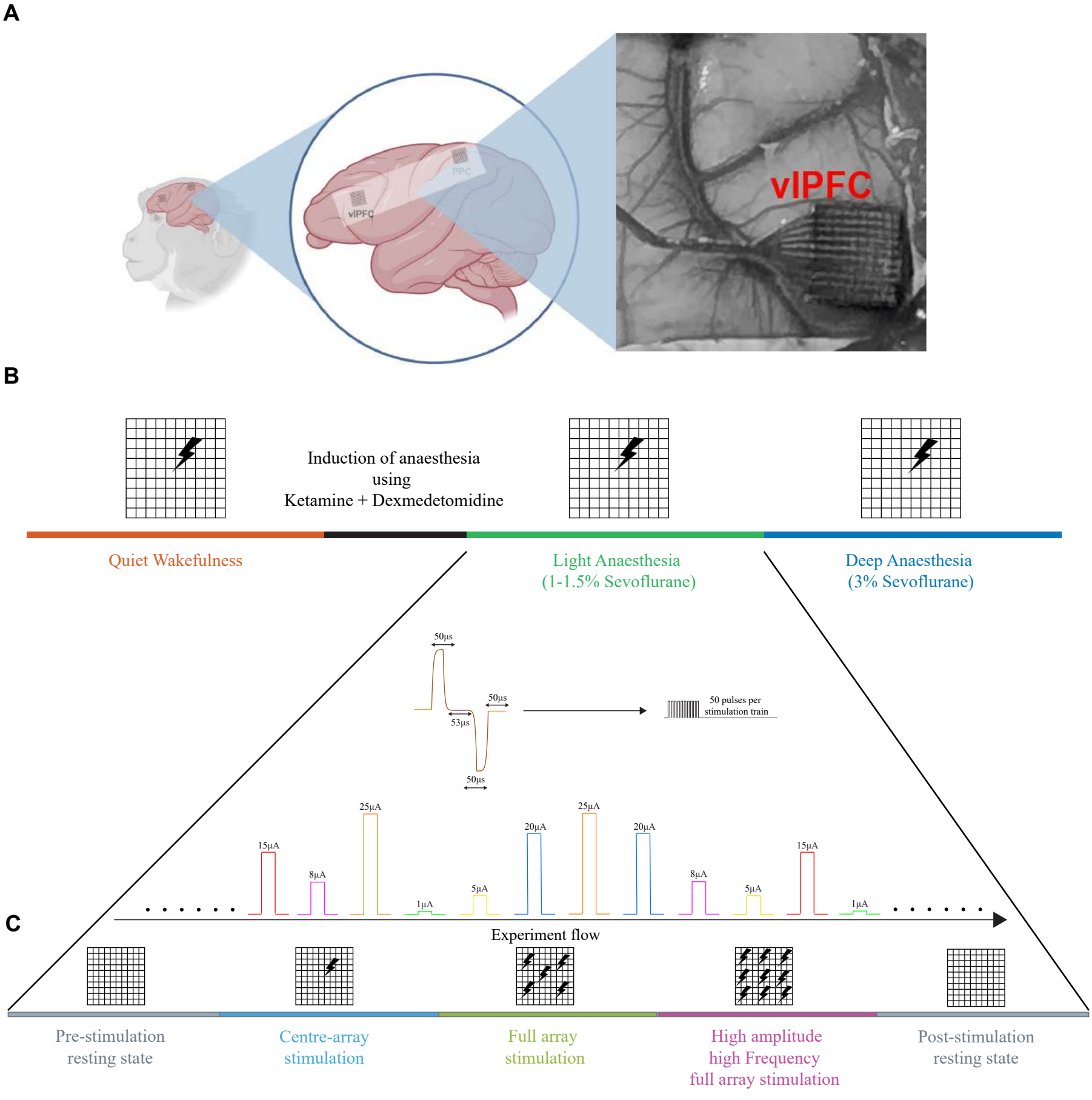
A
vlPFC
PPC
vlPFC
B
Induction of anaesthesia
using
Ketamine + Dexmedetomidine
Quiet Wakefulness
Light Anaesthesia
(1-1.5% Sevoflurane)
Deep Anaesthesia
(3% Sevoflurane)
50µs
53µs
50µs
50µs
50 pulses per
stimulation train
15µA
8µA
25µA
1µA
5µA
20µA
25µA
20µA
8µA
5µA
15µA
1µA
C
Experiment flow
Pre-stimulation
resting state
Centre-array
stimulation
Full array
stimulation
High amplitude
high Frequency
full array stimulation
Post-stimulation
resting state

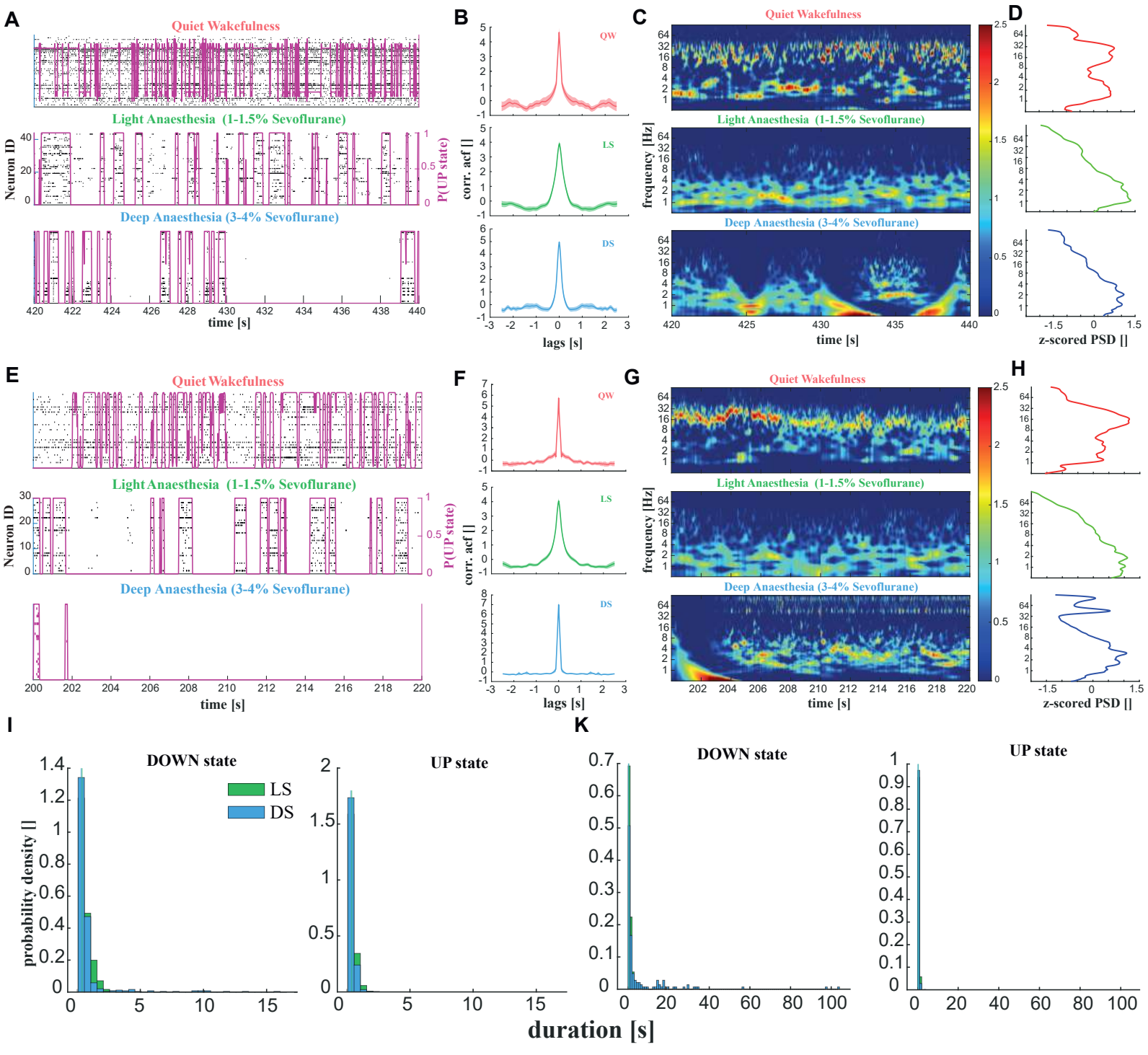
A
Quiet Wakefulness
Light Anaesthesia (1-1.5% Sevoflurane)
Deep Anaesthesia (3-4% Sevoflurane)
Neuron ID
P(UP state)
time [s]
B
QW
LS
DS
corr. acf []
lags [s]
C
Quiet Wakefulness
Light Anaesthesia (1-1.5% Sevoflurane)
Deep Anaesthesia (3-4% Sevoflurane)
frequency [Hz]
time [s]
D
z-scored PSD []
E
Quiet Wakefulness
Light Anaesthesia (1-1.5% Sevoflurane)
Deep Anaesthesia (3-4% Sevoflurane)
Neuron ID
P(UP state)
time [s]
F
QW
LS
DS
corr. acf []
lags [s]
G
Quiet Wakefulness
Light Anaesthesia (1-1.5% Sevoflurane)
Deep Anaesthesia (3-4% Sevoflurane)
frequency [Hz]
time [s]
H
z-scored PSD []
I
DOWN state
UP state
LS
DS
probability density []
K
DOWN state
UP state
duration [s]

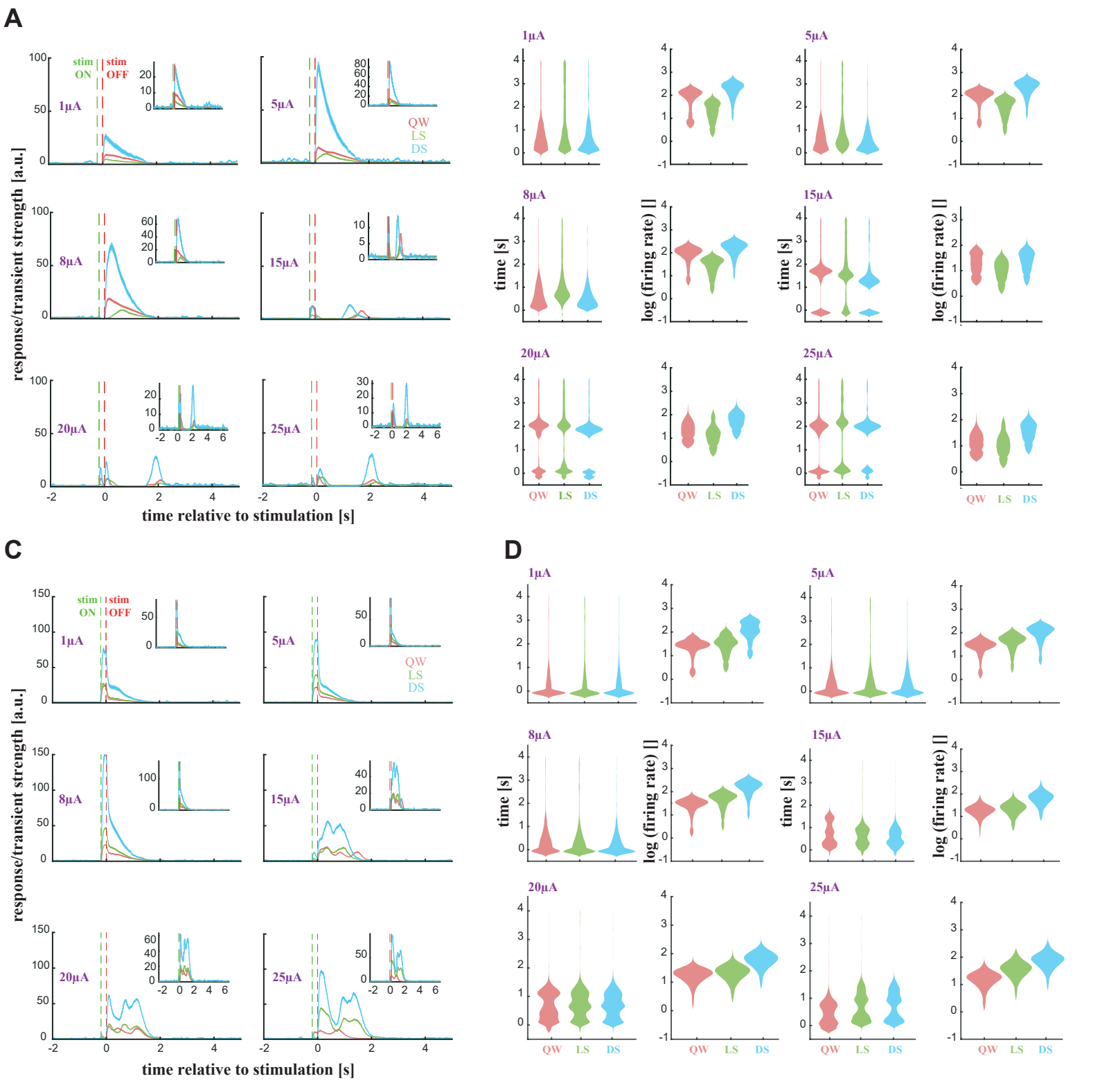
A
C
D
stim ON
stim OFF
1μA
5μA
8μA
15μA
20μA
25μA
QW
LS
DS
response/transient strength [a.u.]
time relative to stimulation [s]
time [s]
log (firing rate) []

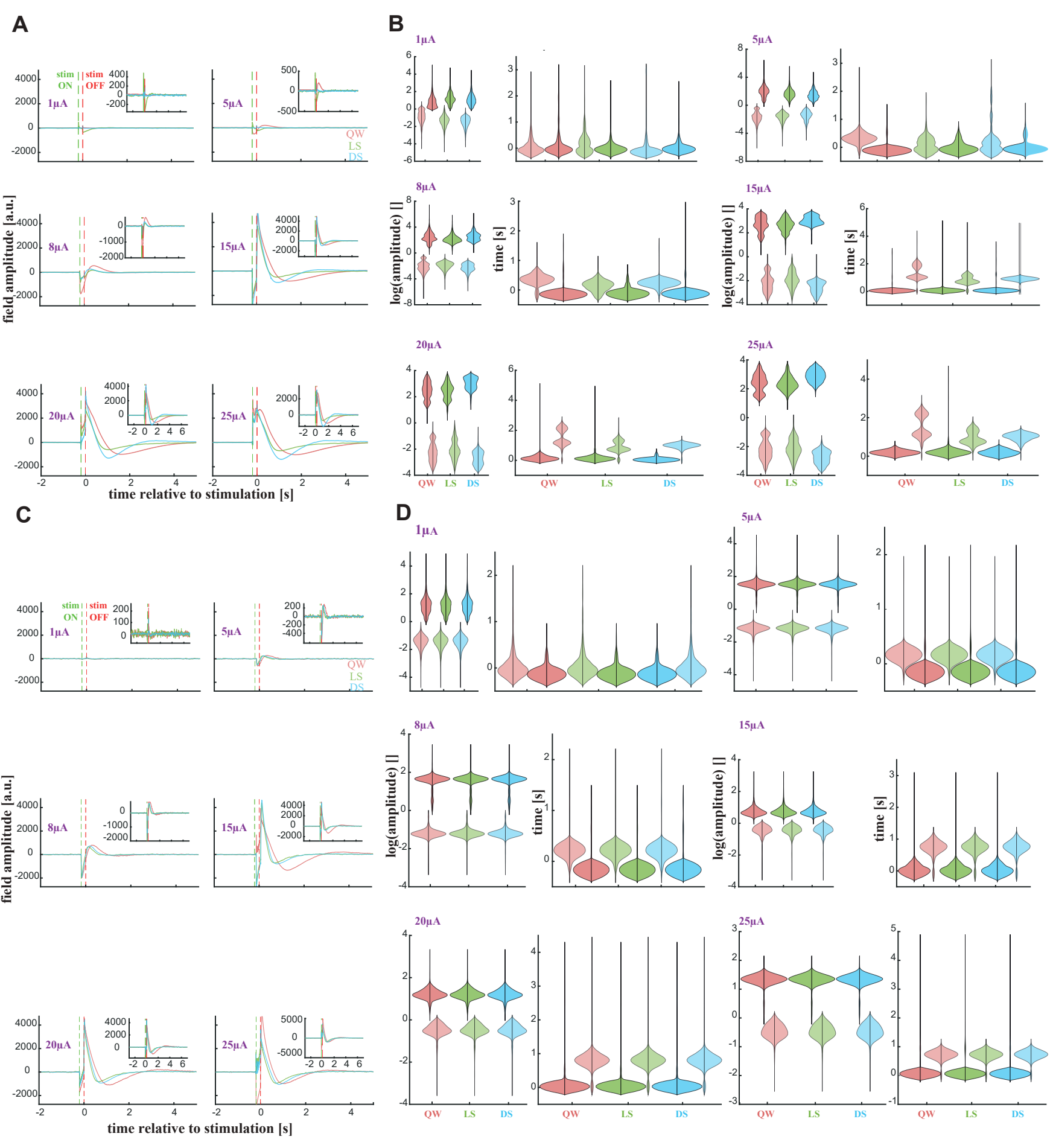
A
B
C
D
stim ON
stim OFF
1µA
5µA
8µA
15µA
20µA
25µA
QW
LS
DS
field amplitude [a.u.]
time relative to stimulation [s]
log(amplitude) []
time [s]

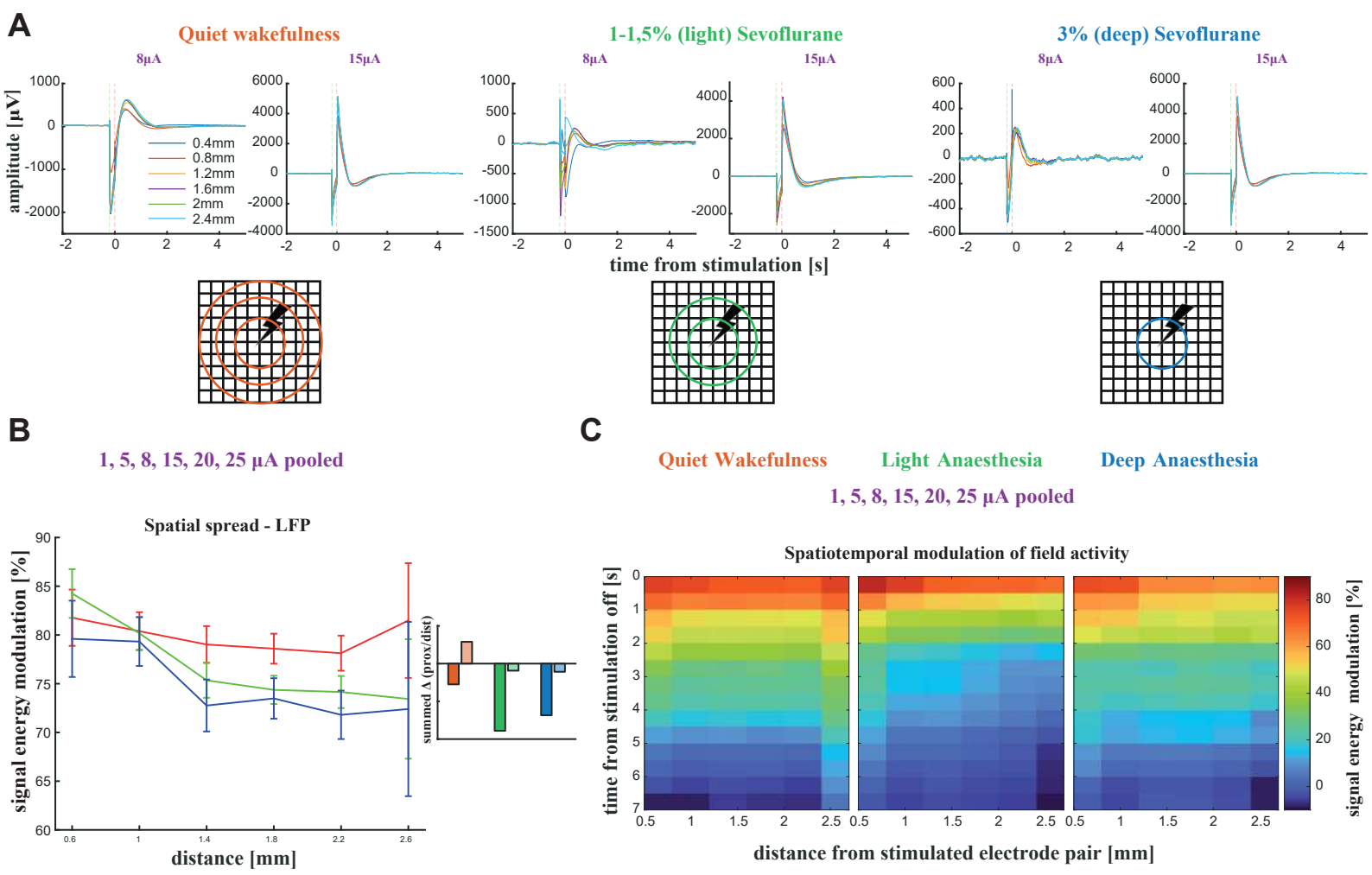
A
Quiet wakefulness
1-1,5% (light) Sevoflurane
3% (deep) Sevoflurane
8µA
15µA
amplitude [µV]
0.4mm
0.8mm
1.2mm
1.6mm
2mm
2.4mm
time from stimulation [s]
B
1, 5, 8, 15, 20, 25 µA pooled
Spatial spread - LFP
signal energy modulation [%]
distance [mm]
summed Δ (prox/dist)
C
Quiet Wakefulness
Light Anaesthesia
Deep Anaesthesia
1, 5, 8, 15, 20, 25 µA pooled
Spatiotemporal modulation of field activity
time from stimulation off [s]
distance from stimulated electrode pair [mm]
signal energy modulation [%]

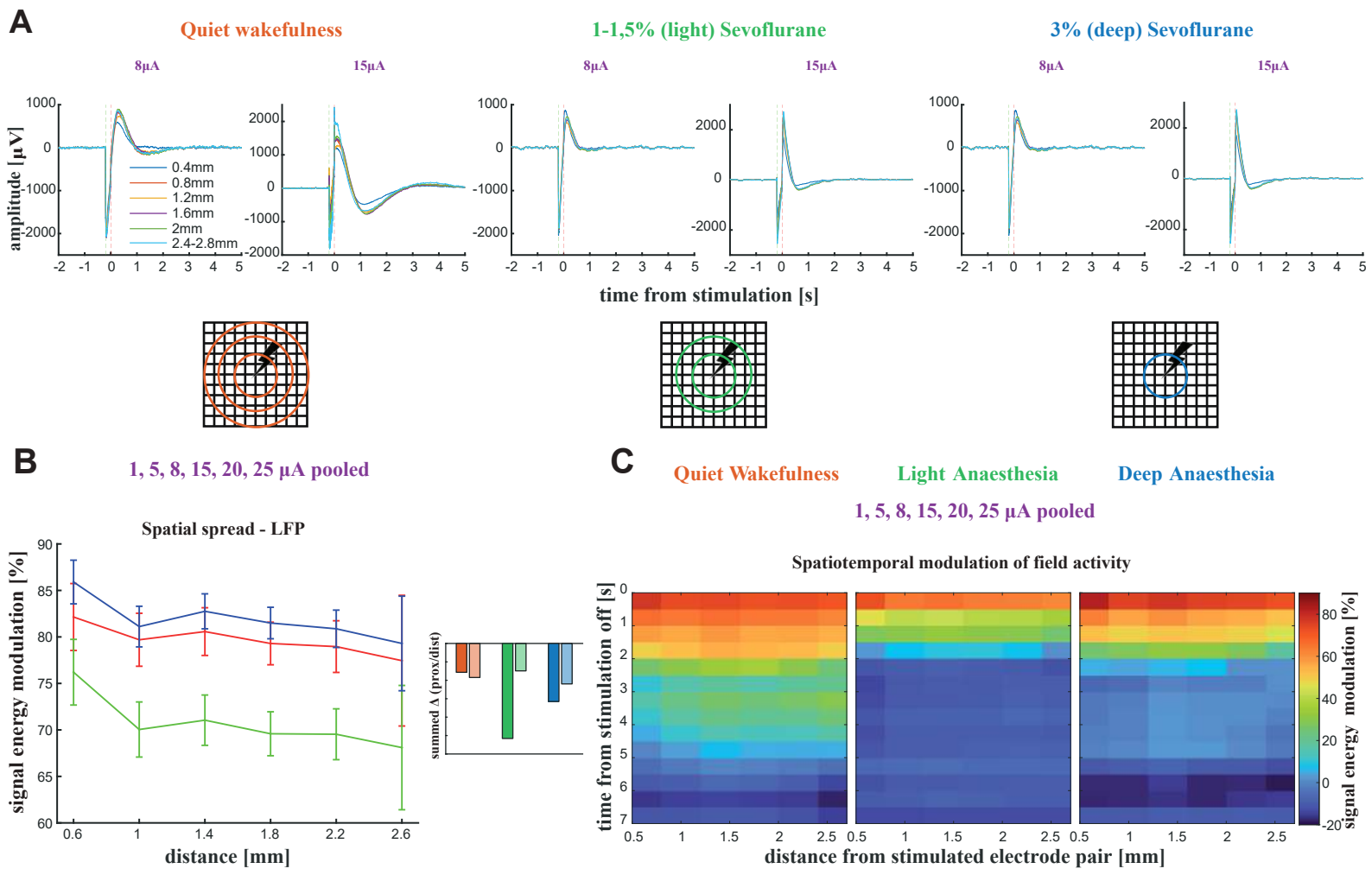
A
Quiet wakefulness
1-1,5% (light) Sevoflurane
3% (deep) Sevoflurane
8µA
15µA
amplitude [µV]
0.4mm
0.8mm
1.2mm
1.6mm
2mm
2.4-2.8mm
time from stimulation [s]
B
1, 5, 8, 15, 20, 25 µA pooled
Spatial spread - LFP
signal energy modulation [%]
distance [mm]
summed Δ (prox/dist)
C
Quiet Wakefulness
Light Anaesthesia
Deep Anaesthesia
1, 5, 8, 15, 20, 25 µA pooled
Spatiotemporal modulation of field activity
time from stimulation off [s]
distance from stimulated electrode pair [mm]
signal energy modulation [%]